Evolution of Microbial Growth Traits Under Serial Dilution

Jie Lin,* Michael Manhart,†,‡ and Ariel Amir*,1

*John A. Paulson School of Engineering and Applied Sciences, Harvard University, Cambridge, Massachusetts 02138, †Department of Chemistry and Chemical Biology, Harvard University, Cambridge, Massachusetts 02138, and ‡Institute of Integrative Biology, ETH Zurich, 8092 Zurich, Switzerland

ORCID IDs: 0000-0002-2027-4661 (J.L.); 0000-0003-3791-9056 (M.M.); 0000-0003-2611-0139 (A.A.)

ABSTRACT Selection of mutants in a microbial population depends on multiple cellular traits. In serial-dilution evolution experiments, three key traits are the lag time when transitioning from starvation to growth, the exponential growth rate, and the yield (number of cells per unit resource). Here, we investigate how these traits evolve in laboratory evolution experiments using a minimal model of population dynamics, where the only interaction between cells is competition for a single limiting resource. We find that the fixation probability of a beneficial mutation depends on a linear combination of its growth rate and lag time relative to its immediate ancestor, even under clonal interference. The relative selective pressure on growth rate and lag time is set by the dilution factor; a larger dilution factor favors the adaptation of growth rate over the adaptation of lag time. The model shows that yield, however, is under no direct selection. We also show how the adaptation speeds of growth and lag depend on experimental parameters and the underlying supply of mutations. Finally, we investigate the evolution of covariation between these traits across populations, which reveals that the population growth rate and lag time can evolve a nonzero correlation even if mutations have uncorrelated effects on the two traits. Altogether these results provide useful guidance to future experiments on microbial evolution.

KEYWORDS Microbial evolution; fixation probability; adaptation rateUS National Institutes of HealthGM116217Swiss National Science FoundationPZ00P3_180147National Science Foundation CAREER1752024Harvard Dean's Competitive FundHarvard's Materials Research and Engineering CenterDMR-1420570

LABORATORY evolution experiments in microbes have provided insight into many aspects of evolution (Elena and Lenski 2003; Barrick and Lenski 2013; Desai 2013), such as the speed of adaptation (Wiser *et al.* 2013), the nature of epistasis (Kryazhimskiy *et al.* 2014), the distribution of selection coefficients from spontaneous mutations (Levy *et al.* 2015), mutation rates (Wielgoss *et al.* 2011), the spectrum of adaptive genomic variants (Barrick *et al.* 2009), and the preponderance of clonal interference (Lang *et al.* 2013). Despite this progress, links between the selection of mutations and their effects on specific cellular traits have remained poorly characterized. Growth traits, such as the lag time when transitioning from starvation to growth, the exponential growth rate, and the yield (resource efficiency), are ideal candidates for investigating this question. Their association with growth means they have relatively direct connections to selection and population dynamics. Furthermore, high-throughput techniques can measure these traits for hundreds of genotypes and environments (Levin-Reisman *et al.* 2010; Warringer *et al.* 2011; Zackrisson *et al.* 2016; Ziv *et al.* 2017). Numerous experiments have shown that single mutations can be pleiotropic, affecting multiple growth traits simultaneously (Fitzsimmons *et al.* 2010; Adkar *et al.* 2017). More recent experiments have even measured these traits at the single-cell level, revealing substantial nongenetic heterogeneity (Levin-Reisman *et al.* 2010; Ziv *et al.* 2013, 2017). Several evolution experiments have found widespread evidence of adaptation in these traits (Vasi *et al.* 1994; Novak *et al.* 2006; Reding-Roman *et al.* 2017; Li *et al.* 2018). This data altogether indicates that covariation in these traits is pervasive in microbial populations.

doi: https://doi.org/10.1534/genetics.120.303149
Manuscript received February 24, 2020; accepted for publication April 27, 2020; published Early Online April 5, 2020.
Available freely online through the author-supported open access option.
Supplemental material available at figshare: https://doi.org/10.25386/genetics.12194754.
[1]Corresponding author: Harvard University, 29 Oxford St., Cambridge, MA 02138. E-mail: arielamir@seas.harvard.edu

There have been a few previous attempts to develop quantitative models to describe evolution of these traits. For example, Vasi *et al.* (1994) considered data after 2000 generations of evolution in *Escherichia coli* to estimate how much adaptation was attributable to different growth traits. Smith (2011) developed a mathematical model to study how different traits would allow strains to either fix, go extinct, or coexist. Wahl and Zhu (2015) studied the fixation probability of mutations affecting different growth traits separately (nonpleiotropic), especially to identify which traits were most likely to acquire fixed mutations and the importance of mutation occurrence time and dilution factor. However, simple quantitative results that can be used to interpret experimental data have remained lacking. More recent work (Manhart *et al.* 2018; Manhart and Shakhnovich 2018) derived a quantitative relation between growth traits and selection, showing that selection consists of additive components on the lag and growth phases. However, this did not address the consequences of this selection for evolution, especially the adaptation of trait covariation.

In this work, we investigate a minimal model of evolutionary dynamics in which cells interact only by competition for a single limiting resource. We find that the fixation probability of a mutation is accurately determined by a linear combination of its change in growth rate and change in lag time relative to its immediate ancestor, rather than depending on the precise combination of traits; the relative weight of these two components is determined by the dilution factor. Yield, on the other hand, is under no direct selection. This is true even in the presence of substantial clonal interference, where the mutant's immediate ancestor may have a large fitness difference from the population mean. We provide quantitative predictions for the speed of adaptation of growth rate and lag time as well as their evolved covariation. Specifically, we find that even in the absence of an intrinsic correlation between growth and lag due to mutations, these traits can evolve a nonzero correlation due to selection and variation in number of fixed mutations.

Materials and Methods

Model of population dynamics

We consider a model of asexual microbial cells in a well-mixed batch culture, where the only interaction between different strains is competition for a single limiting resource (Manhart *et al.* 2018; Manhart and Shakhnovich 2018). Each strain k is characterized by a lag time L_k, growth rate r_k, and yield Y_k (see Figure 1A for a two-strain example). Here the yield is the number of cells per unit resource (Vasi *et al.* 1994), so that $N_k(t)/Y_k$ is the amount of resources consumed by time t by strain k, where $N_k(t)$ is the number of cells of strain k at time t. We define R to be the initial amount of the limiting resource and assume different strains interact only by competing for the limiting resource; their growth traits are the same as when they grow independently. When the population has consumed all of the initial resource, the population reaches stationary phase with constant size. The saturation time t_c at which this occurs is determined by $\sum_{\text{strain } k} N_k(t_c)/Y_k = R$, which we can write in terms of the growth traits as

$$\sum_{\text{strain } k} \frac{N_0 x_k e^{r_k(t_c - L_k)}}{Y_k} = R, \tag{1}$$

where N_0 is the total population size and x_k is the frequency of each strain k at the beginning of the growth cycle. In Equation 1, we assume the time t_c is longer than each strain's lag time L_k. Note that some of our notation differs from related models in previous work, some of which used g for growth rate and λ for lag time (Manhart *et al.* 2018), while others used λ for growth rate (Lin and Amir 2017). Although it is possible to extend the model to account for additional growth traits such as a death rate or lag and growth on secondary resources, here we focus on the minimal set of traits most often measured in microbial phenotyping experiments (Novak *et al.* 2006; Fitzsimmons *et al.* 2010; Levin-Reisman *et al.* 2010; Warringer *et al.* 2011; Jasmin and Zeyl 2012; Ziv *et al.* 2013; Zackrisson *et al.* 2016; Adkar *et al.* 2017).

We define the selection coefficient between each pair of strains as the change in their log-ratio over the complete growth cycle (Chevin 2011; Good *et al.* 2017):

$$\begin{aligned} s_{ij} &= \ln\left(\frac{N_i^{\text{final}}}{N_j^{\text{final}}}\right) - \ln\left(\frac{N_i^{\text{initial}}}{N_j^{\text{initial}}}\right) \\ &= r_i(t_c - L_i) - r_j(t_c - L_j), \end{aligned} \tag{2}$$

where N_i^{initial} is the population size of strain i at the beginning of the growth cycle and N_i^{final} is the population size of strain i at the end. After the population reaches stationary phase, it is diluted by a factor of D into a fresh medium with amount R of the resource, and the cycle repeats (Figure 1A). We assume the population remains in the stationary phase for a sufficiently short time, such that we can ignore death and other dynamics during this phase (Finkel 2006; Avrani *et al.* 2017).

Over many cycles of growth, as would occur in a laboratory evolution experiment (Lenski *et al.* 1991; Elena and Lenski 2003; Good *et al.* 2017), the population dynamics of this system are characterized by the set of frequencies x_k for all strains as well as the matrix of selection coefficients s_{ij} and the total population size N_0 at the beginning of each cycle. In Supplemental Material, Supplemental Methods (sections I, II, and III), we derive explicit equations for the deterministic dynamics of these quantities over multiple cycles of growth for an arbitrary number of strains. In the case of two strains, such as a mutant and a wild type, the selection coefficient is approximately

$$s \approx \gamma \ln D - \omega, \tag{3}$$

where $\gamma = (r_2 - r_1)/r_1$ is the growth rate of the mutant relative to the wild type and $\omega = (L_2 - L_1)r_1$ is the relative lag

time. The approximation is valid as long as the growth rate difference between the mutant and the wild type is small (Supplemental Methods, section IV), which is true for most single mutations (Chevereau *et al.* 2015; Levy *et al.* 2015). This equation shows that the growth phase and the lag phase make distinct additive contributions to the total selection coefficient, with the dilution factor D controlling their relative magnitudes (Figure 1B). This is because a larger dilution factor will increase the amount of time the population grows exponentially, hence increasing selection on growth rate. Neutral coexistence between multiple strains is therefore possible if these two selection components balance ($s = 0$), although it requires an exact tuning of the growth traits with the dilution factor (Supplemental Methods, section III) (Manhart *et al.* 2018; Manhart and Shakhnovich 2018). With a fixed dilution factor D, the population size N_0 at the beginning of each growth cycle changes according to (Supplemental Methods, section I)

$$N_0 = \frac{R\bar{Y}}{D}, \tag{4}$$

where $\bar{Y} = (\sum_{\text{strain } k} x_k/Y_k)^{-1}$ is the effective yield of the whole population in the current growth cycle. In this manner the ratio R/D sets the bottleneck size of the population, which for serial dilution is approximately the effective population size (Lenski *et al.* 1991), and therefore determines the strength of genetic drift.

Model of evolutionary dynamics

We now consider the evolution of a population as new mutations arise that alter growth traits. We start with a wild-type population having lag time $L_0 = 100$ and growth rate $r_0 = (\ln 2)/60 \approx 0.012$, which are roughly consistent with *E. coli* parameters, where time is measured in minutes (Lenski *et al.* 1991; Vasi *et al.* 1994); we set the wild-type yield to be $Y_0 = 1$ without loss of generality. As in experiments, we vary the dilution factor D and the amount of resources R, which control the relative selection on growth *vs.* lag (set by D, Equation 3) and the effective population size (set by R/D, Equation 4). We also set the initial population size of the first cycle to $N_0 = RY_0/D$.

The population grows according to the dynamics in Figure 1A. Each cell division can generate a new mutation with probability $\mu = 10^{-6}$; note that this rate is only for mutations altering growth traits, and therefore it is lower than the rate of mutations anywhere in the genome. We generate a random waiting time τ_k for each strain k until the next mutation with instantaneous rate $\mu r_k N_k(t)$. When a mutation occurs, the growth traits for the mutant are drawn from a distribution $p_{\text{mut}}(r_2, L_2, Y_2 | r_1, L_1, Y_1)$, where r_1, L_1, Y_1 are the growth traits for the background strain on which the new mutation occurs and r_2, L_2, Y_2 are the traits for the new mutant. Note that since mutations only arise during the exponential growth phase, beneficial or deleterious effects on lag time are not realized until the next growth cycle (Li *et al.* 2018). After the growth cycle ceases (once the resource is exhausted according to Equation 1), we randomly choose cells, each with probability $1/D$, to form the population for the next growth cycle.

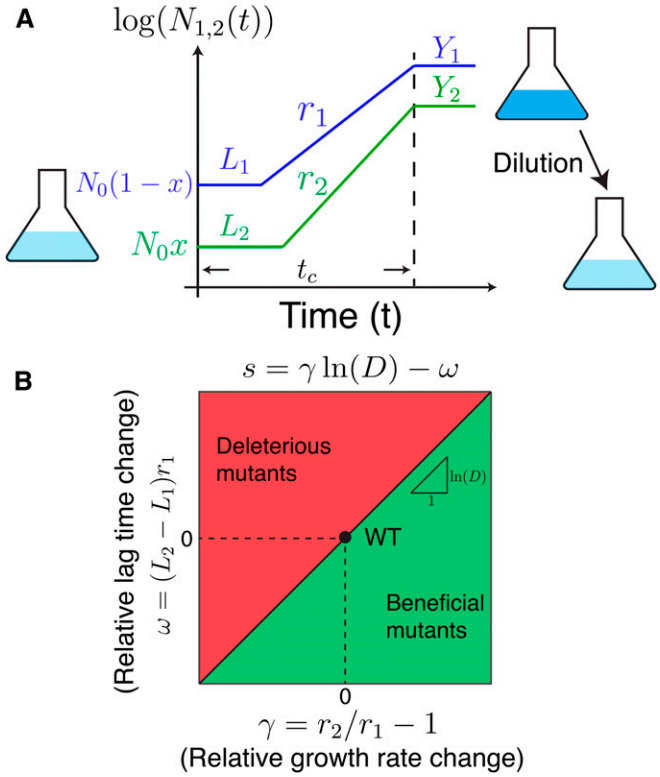

Figure 1 Model of selection on multiple microbial growth traits. (A) Simplified model of microbial population growth characterized by three traits: lag time L, growth rate r, and yield Y. The total initial population size is N_0 and the initial frequency of the mutant (strain 2) is x. After the whole population reaches stationary phase (time t_c), the population is diluted by a factor D into fresh media, and the cycle starts again. (B) Phase diagram of selection on mutants in the space of their growth rate $\gamma = r_2/r_1 - 1$ and lag time $\omega = (L_2 - L_1)r_1$ relative to wild type. The slope of the diagonal line is ln D.

We will assume mutational effects are not epistatic and scale with the trait values of the background strain, so that $p_{\text{mut}}(r_2, L_2, Y_2 | r_1, L_1, Y_1) = p_{\text{mut}}(\gamma, \omega, \delta)$, where $\gamma = (r_2 - r_1)/r_1$, $\omega = (L_2 - L_1)r_1$, and $\delta = (Y_2 - Y_1)/Y_1$ (Supplemental Methods, section V). Since our primary goal is to scan the space of possible mutations, we focus on uniform distributions of mutational effects where $-0.02 < \gamma < 0.02$, $-0.05 < \omega < 0.05$, and $-0.02 < \delta < 0.02$. In the Supplemental Methods, we extend our main results to the case of Gaussian distributions (section V) as well as an empirical distribution of mutational effects based on single-gene deletions in *E. coli* (section VI) (Campos *et al.* 2018).

Data availability

Data and codes are available upon request. File S1 contains the Supplemental Methods. File S2 contains data of growth traits presented in Figure S3. Supplemental material available at figshare: https://doi.org/10.25386/genetics.12194754.

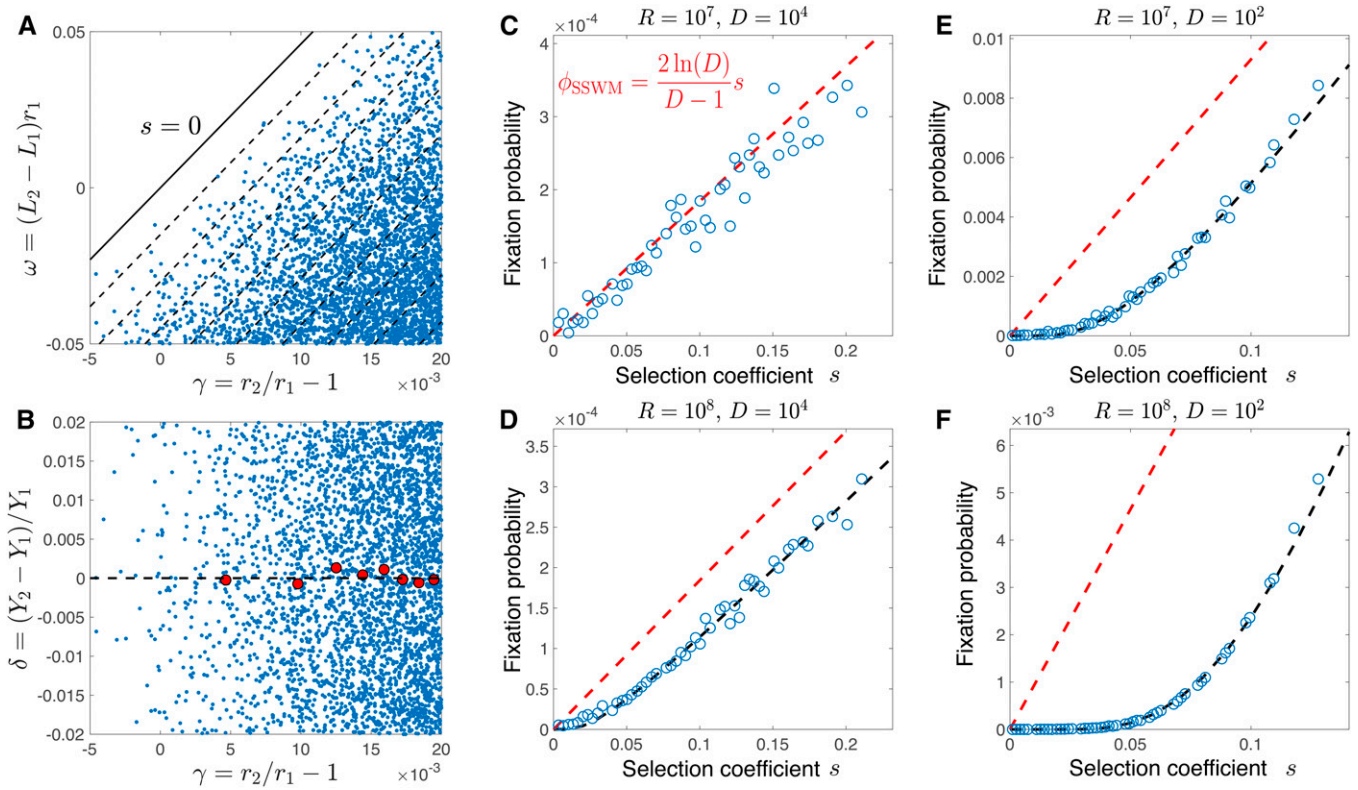

Figure 2 Selection coefficient determines fixation probability. (A) The relative growth rates γ and the relative lag times ω of fixed mutations against their background strain. Dashed lines mark contours of constant selection coefficient with interval $\Delta s = 0.015$ while the solid line marks $s = 0$. (B) Same as A, but for relative growth rate γ and the relative yield δ. The red dots mark the relative yield of fixed mutations averaged over binned values of the relative growth rate γ. In A and B, $D = 10^2$ and $R = 10^7$. (C, D, E, and F) Fixation probability of mutations against their selection coefficients for different amounts of resource R and dilution factors D as indicated in the titles. The red dashed line shows the fixation probability predicted in the SSWM regime (Equation 5), while the black line shows a numerical fit of the data points to Equation 6 with parameters $A = 0.0017$ and $B = 0.0421$ in D, $A = 0.1145$ and $B = 0.0801$ in E, and $A = 0.2121$ and $B = 0.2192$ in F. In all panels mutations randomly arise from a uniform distribution p_{mut} with $-0.02 < \gamma < 0.02$, $-0.05 < \omega < 0.05$, and $-0.02 < \delta < 0.02$.

Results

Fixation of mutations

We first consider the fixation statistics of new mutations in our model. In Figure 2A we show the relative growth rates γ and the relative lag times ω of fixed mutations against their background strains, along with contours of constant selection coefficient s from Equation 3. As expected, fixed mutations either increase growth rate $(\gamma > 0)$, decrease lag time $(\omega < 0)$, or both. In contrast, the yield of fixed mutations is the same as the ancestor on average (Figure 2B); indeed, the selection coefficient in Equation 3 does not depend on the yields. If a mutation arises with significantly higher or lower yield than the rest of the population, the bottleneck population size N_0 immediately adjusts to keep the overall fold-change of the population during the growth cycle fixed to the dilution factor D (Equation 4). Therefore mutations that significantly change yield have no effect on the overall population dynamics.

Figure 2A also suggests that the density of fixed mutations in the growth-lag trait space depends solely on their selection coefficients, rather than the precise combination of traits, as long as other parameters such as the dilution factor D, the total amount of resource R, and the distribution of mutational effects are held fixed. Mathematically, this means that the fixation probability $\phi(\gamma, \omega)$ of a mutation with growth effect γ and lag effect ω can be expressed as $\phi(\gamma, \omega) = \phi(\gamma \ln D - \omega) \equiv \phi(s)$. To test this, we discretize the scatterplot of Figure 2A and compute the fixation probabilities of mutations as functions of γ and ω (Supplemental Methods, section VII). We then plot the resulting fixation probabilities of mutations as functions of their selection coefficients calculated by Equation 3 (Figure 2, C–F). We test the dependence of the fixation probability on the selection coefficient over a range of population dynamics regimes by varying the dilution factor D and the amount of resources R.

For small populations, mutations generally arise and either fix or go extinct one at a time, a regime known as strong-selection weak-mutation (SSWM) (Gillespie 1984). In this case, we expect the fixation probability of a beneficial mutation with selection coefficient $s > 0$ to be (Wahl and Gerrish 2001; Wahl and Zhu 2015; Guo *et al.* 2019)

$$\phi_{\mathrm{SSWM}}(s) = \frac{2 \ln D}{D-1} s. \tag{5}$$

This is similar to the standard Wright–Fisher fixation probability of $2s$ (Crow and Kimura 1970), but with a different prefactor due to averaging over the different times in the exponential growth phase at which the mutation can arise (Supplemental Methods, section VIII). Indeed, we see this predicted dependence matches the simulation results for the small population size of $N_0 \sim R/D = 10^3$ (Figure 2C).

For larger populations, multiple beneficial mutations will be simultaneously present in the population and interfere with each other, an effect known as clonal interference (Gerrish and Lenski 1998; Desai and Fisher 2007; Schiffels *et al.* 2011; Good *et al.* 2012; Fisher 2013; Good and Desai 2014). Our simulations show that, as for the SSWM case, the fixation probability depends only on the selection coefficient (Equation 3) relative to the mutation's immediate ancestor and not on the individual combination of mutant traits (Figure 2, D–F), with all other population parameters held constant. Previous work has determined the dependence of the fixation probability on the selection coefficient under clonal interference using various approximations (Gerrish and Lenski 1998; Schiffels *et al.* 2011; Good *et al.* 2012; Fisher 2013). Here, we focus on an empirical relation based on (Gerrish and Lenski 1998)

$$\phi_{\mathrm{CI}}(s) = A s e^{-B/s}, \tag{6}$$

where A and B are two constants that depend on other parameters of the population (D, R, and the distribution of mutational effects); we treat these as empirical parameters to fit to the simulation results, although Gerrish and Lenski (1998) predicted $A = 2 \ln D/(D-1)$, *i.e.*, the same constant as in the SSWM case (Equation 5). The $e^{-B/s}$ factor in Equation 6 comes from the probability that no superior beneficial mutations appears before the current mutation fixes. Since the time to fixation scales as $1/s$, we expect the average number of superior mutations to be proportional to $1/s$ (for small s). This approximation holds only for selection coefficients that are not too small and therefore are expected to fix without additional beneficial mutations on the same background; Equation 6 breaks down for weaker beneficial mutations that typically fix by hitchhiking on stronger mutations (Schiffels *et al.* 2011). Nevertheless, Equation 6 matches our simulation results well for a wide range of selection coefficients achieved in our simulations and larger population sizes $N_0 \sim R/D > 10^4$ (Figure 2, D–F). Furthermore, the constant A we fit to the simulation data are indeed close to the predicted value of $2 \ln D/(D-1)$, except in the most extreme case of $N_0 \sim R/D = 10^6$ (Figure 2F).

Altogether, Figure 2 shows that mutations with different effects on cell growth (for example, a mutant that increases the growth rate and a mutant that decreases the lag time) can nevertheless have approximately the same fixation probability as long as their overall effects on selection are the same according to Equation 3. To test the robustness of this result, we verify it for several additional distributions of mutational effects $p_{\mathrm{mut}}(\gamma, \omega, \delta)$ in the Supplemental Methods: a Gaussian distribution of mutational effects, including the presence of correlated mutational effects (Figure S1); a wider distribution of mutational effects with large selection coefficients (Figure S2); and an empirical distribution of mutational effects estimated from single-gene deletions in *E. coli* (Figure S3). In Figure S4A, we further test robustness by using the neutral phenotype (orthogonal to the selection coefficient) to quantify the range of γ and ω trait combinations that nevertheless have the same selection coefficient and fixation probability, and in Figure S4B we show that the selection coefficient on growth alone is insufficient to determine fixation probability.

While the dependence of fixation probability on the selection coefficient is a classic result of population genetics (Hartl and Clark 1997), the existence of a simple relationship here is nontrivial since, strictly speaking, selection in this model is not only frequency-dependent (Manhart *et al.* 2018) (*i.e.*, selection between two strains depends on their frequencies) but also includes higher-order effects (Manhart and Shakhnovich 2018) (*i.e.*, selection between strain 1 and strain 2 is affected by the presence of strain 3). Therefore, in principle, the fixation probability of a mutant may depend on the specific state of the population in which it is present, while the selection coefficient in Equation 3 only describes selection on the mutant in competition with its immediate ancestor. However, we see that, at least for the parameters considered in our simulations, these effects are negligible in determining the eventual fate of a mutation.

Adaptation of growth traits

As Figure 3A shows, many mutations arise and fix over the timescale of our simulations, which lead to predictable trends in the quantitative traits of the population. We first determine the relative fitness of the evolved population at each time point against the ancestral strain by simulating competition between an equal number of evolved and ancestral cells for one cycle, analogous to common experimental measurements (Lenski *et al.* 1991; Elena and Lenski 2003). The resulting fitness trajectories are shown in Figure 3B. To see how different traits contribute to the fitness increase, we also calculate the average population traits at the beginning of each cycle; for instance, the average population growth rate at growth cycle n is $r_{\mathrm{pop}}(n) = \sum_{\mathrm{strain}\ k} r_k x_k(n)$. As expected from Equation 3, the average growth rate increases (Figure 3C) and the average lag time decreases (Figure 3D) for all simulations. In contrast, the average yield evolves without apparent trend (Figure 3E), since Equation 3 indicates no direct selection on yield. We note that, while the cells do not evolve toward lower or higher resource efficiency on average, they do evolve to consume resources more quickly, since the rate of resource consumption (r_k/Y_k for each cell of strain k) depends on both the yield as well as the growth rate. Therefore the saturation time of each growth cycle evolves to

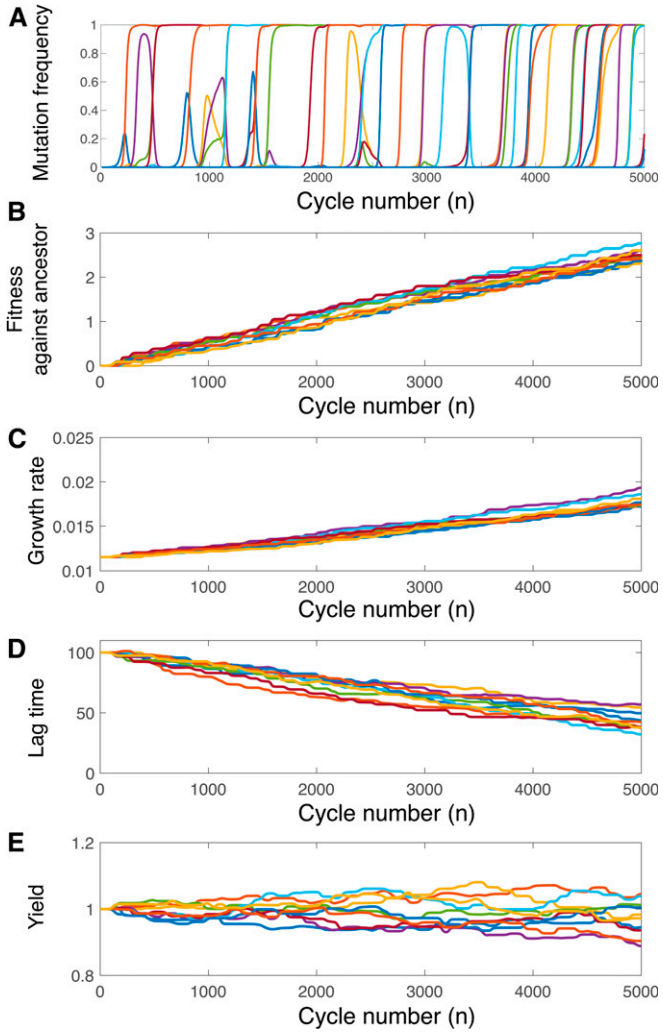

Figure 3 Dynamics of evolving populations. (A) Frequencies of new mutations as functions of the number n of growth cycles. Example trajectories of (B) the fitness of the evolved population relative to the ancestral population, (C) the evolved average growth rate, (D) the evolved average lag time, and (E) the evolved average yield. In all panels the dilution factor is $D = 10^2$, the amount of resource at the beginning of each cycle is $R = 10^7$, and mutations randomly arise from a uniform distribution p_{mut} with $-0.02 < \gamma < 0.02$, $-0.05 < \omega < 0.05$, and $-0.02 < \delta < 0.02$.

be shorter, consistent with recent work from Baake *et al.* (2019).

Figure 3 suggests relatively constant speeds of adaptation for the relative fitness, the average growth rate, and the average lag time. For example, we can calculate the adaptation speed of the average growth rate as the averaged change in the average growth rate per cycle:

$$W_{\text{growth}} = \langle r_{\text{pop}}(n+1) - r_{\text{pop}}(n) \rangle, \tag{7}$$

where the bracket denotes an average over replicate populations and cycle number. In the Supplemental Methods (sections IX and X), we calculate the adaptation speeds of these traits in the SSWM regime to be

$$W_{\text{growth}} = \sigma_\gamma^2 r_0 (\ln D)\left(\frac{\mu R Y_0 \ln D}{D-1}\right),$$
$$W_{\text{lag}} = -\frac{\sigma_\omega^2}{r_0}\left(\frac{\mu R Y_0 \ln D}{D-1}\right), \tag{8}$$
$$W_{\text{fitness}} = \frac{W_{\text{growth}}}{r_0}\ln D - W_{\text{lag}} r_0,$$

where σ_γ and σ_ω are the standard deviations of the underlying distributions of γ and ω for single mutations ($p_{\text{mut}}(\gamma, \omega, \delta)$), r_0 is the ancestral growth rate, and Y_0 is the ancestral yield (we assume the yield does not change on average according to Figure 3E). Furthermore, the ratio of the growth adaptation rate and the lag adaptation rate is independent of the amount of resource and mutation rate in the SSWM regime:

$$\frac{W_{\text{growth}}}{W_{\text{lag}}} = -r_0^2 \frac{\sigma_\gamma^2}{\sigma_\omega^2} \ln D. \tag{9}$$

Equation 8 predicts that the adaptation speeds of the average growth rate, the average lag time, and the relative fitness should all increase with the amount of resources R and decrease with the dilution factor D (for large D); although this prediction assumes the SSWM regime (relatively small $N_0 \sim R/D$), it nevertheless holds across a wide range of R- and D-values (Figure 4, A–C), except for $R = 10^8$ where the speed of fitness increase is nonmonotonic with D (Figure 4C). The predicted adaptation speeds in Equation 8 also quantitatively match the simulated trajectories in the SSWM case (Figure 4, D–F); even outside of the SSWM regime, the relative rate in Equation 9 remains a good prediction at early times (Figure S5).

Evolved covariation between growth traits

We now turn to investigating how the covariation between traits evolves. We have generally assumed that individual mutations have uncorrelated effects on different traits. Campos *et al.* (2018) recently systematically measured the growth curves of the single-gene deletions in *E. coli*. We compute the relative growth rate, lag time, and yield changes for the single-gene deletions compared with the wild type and find that the resulting empirical distribution of relative growth traits changes shows very small correlations between these traits (Figure S3, B and C), consistent with our assumptions. We note that these measurements, however, are subject to significant noise (Supplemental Methods, section VI), and therefore any conclusions ultimately require verification by further experiments.

Even in the absence of mutational correlations, selection may induce a correlation between these traits in evolved populations. In Figure 5A, we schematically depict how the raw variation of traits from mutations is distorted by selection and fixation of multiple mutations. Specifically, for a single fixed mutation, selection induces a positive (*i.e.*, antagonistic) correlation between the relative growth rate change and

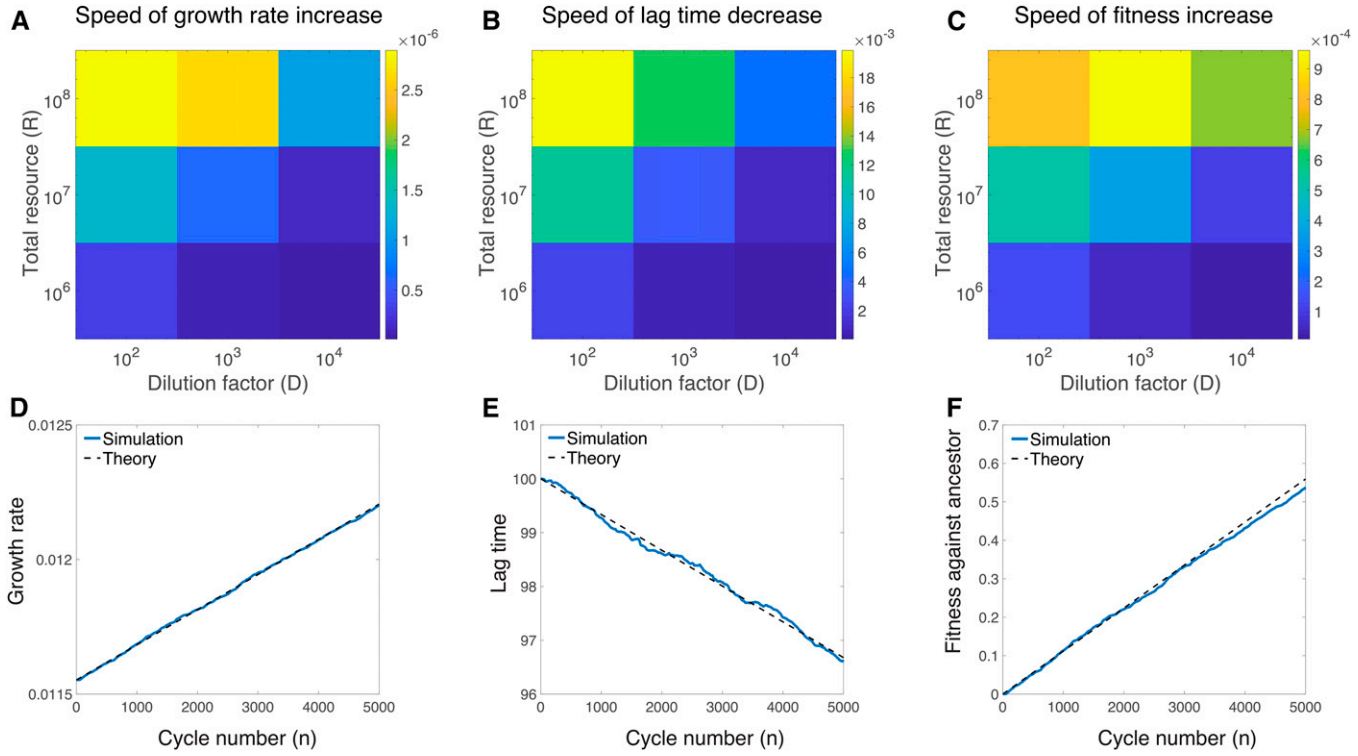

Figure 4 Speed of adaptation. The average per-cycle adaptation speed of (A) the average growth rate, (B) the average lag time, and (C) the fitness relative to the ancestral population as functions of the dilution factor D and total amount of resources R. The adaptation speeds are averaged over growth cycles and independent populations. (D) The average growth rate, (E) the average lag time, and (F) the fitness relative to the ancestral population as functions of the number n of growth cycles. The dilution factor is $D = 10^4$ and the total resource is $R = 10^7$, so the population is in the SSWM regime. The blue solid lines are simulation results, while the dashed lines show the mathematical predictions in Equation 8. All panels show averages over 500 independent simulated populations, with mutations randomly arising from a uniform distribution p_{mut} with $-0.02 < \gamma < 0.02$, $-0.05 < \omega < 0.05$, and $-0.02 < \delta < 0.02$.

the relative lag time change. Figure 2A shows this for single fixed mutations, while Figure 5, B and C shows this positive correlation between the average growth rate and the average lag time across populations that have accumulated the same number of fixed mutations. For populations in the SSWM regime with the same number of fixed mutations, the Pearson correlation coefficient between the average growth rate and the average lag time across populations is approximately equal to the covariation of the relative growth rate change γ and the relative lag time change ω for a single fixed mutation:

$$\rho_{\text{fixed}} \approx \frac{\langle \gamma\omega \rangle_{\text{fixed}} - \langle \gamma \rangle_{\text{fixed}} \langle \omega \rangle_{\text{fixed}}}{\sqrt{\left(\langle \gamma^2 \rangle_{\text{fixed}} - \langle \gamma \rangle_{\text{fixed}}^2 \right) \left(\langle \omega^2 \rangle_{\text{fixed}} - \langle \omega \rangle_{\text{fixed}}^2 \right)}}, \quad (10)$$

where $\langle \cdot \rangle_{\text{fixed}}$ is an average over the distribution of single fixed mutations (Supplemental Methods, section IX). We can explicitly calculate this quantity in the SSWM regime, which confirms that it is positive for uncorrelated mutational effects with uniform or Gaussian distributions (Supplemental Methods, section XI).

However, in evolution experiments we typically observe populations at a particular snapshot in time, such that the populations may have a variable number of fixed mutations but the same number of total mutations that arose and either fixed or went extinct (since the number of total arising mutations is very large, we neglect its fluctuation across populations). Interestingly, the variation in number of fixed mutations at a snapshot in time causes the distribution of growth rates and lag times across populations to stretch into a negative correlation; this is an example of Simpson's paradox from statistics (Simpson 1951). Figure 5A shows this effect schematically, while Figure 5, D and E show explicit results from simulations. An intuitive way to understand the evolved negative correlation is to approximate the effects of all fixed mutations as deterministic, so that each fixed mutation increases the average growth rate and decreases the average lag time by the same amount. Therefore, populations with a higher average growth rate must have a larger number of fixed mutations and thus also a shorter average lag time, leading to a negative correlation between the average growth rates and the average lag times. In the Supplemental Methods (section XI), we calculate this evolved Pearson correlation coefficient across populations in the SSWM regime to be approximately

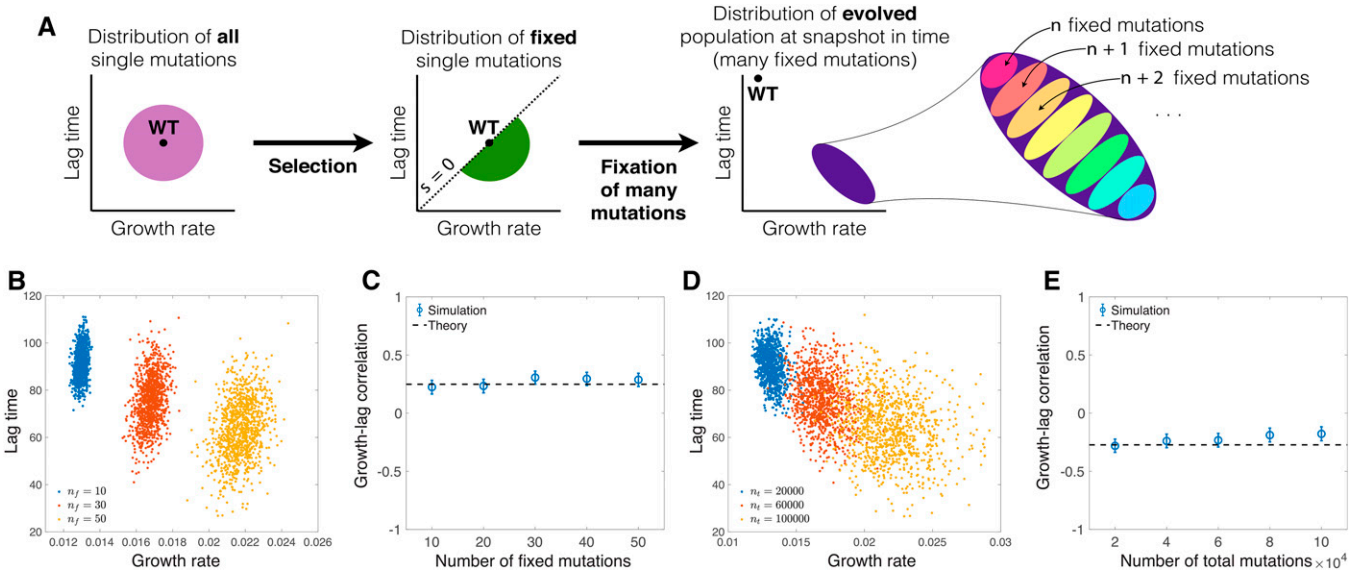

Figure 5 Evolved patterns of covariation among growth traits. (A) Schematic of how selection and fixation of multiple mutations shape the observed distribution of traits. The sign of the Pearson correlation coefficient between the average growth rate and lag time depends on whether we consider an ensemble of populations with the same number of fixed mutations or the same number of total mutation events. (B) Distribution of average growth rate and lag time for 1000 independent populations with the same number of fixed mutations. Each color corresponds to a different number of fixed mutations (n_f) indicated in the legend. (C) Pearson correlation coefficient of growth rate and lag time for distributions in B, as a function of the number of fixed mutations. The dashed line is the prediction from Equation 10. (D) Same as B, except each color corresponds to a set of populations at a snapshot in time with the same number of total mutation events. Each color corresponds to a different number of total mutations events (n_t) indicated in the legend. (E) Same as C, but for the set of populations shown in D. The dashed line is the prediction from Equation 11. In C and E, the error bars represent 95% confidence intervals. In B–E, we simulate the SSWM regime by introducing random mutations one by one and determining their fixation from Equation 5 with $D = 10^3$.

$$\rho_{\text{evo}} \approx \frac{\langle \gamma\omega \rangle_{\text{fixed}}}{\sqrt{\langle \gamma^2 \rangle_{\text{fixed}} \langle \omega^2 \rangle_{\text{fixed}}}}. \tag{11}$$

That is, the correlation of traits across populations with multiple mutations is still a function of the distribution of single fixed mutations, but it is not equal to the correlation of single fixed mutations (Equation 10). In the Supplemental Methods (section XI), we explicitly calculate ρ_{evo} in the SSWM regime for uncorrelated uniform and Gaussian distributions of mutational effects, which shows that it is negative. Furthermore, we prove that it must always be negative for any symmetric and uncorrelated distribution $p_{\text{mut}}(\gamma, \omega)$ (Supplemental Methods, section IX).

The predicted correlations in Equations 10 and 11 quantitatively match the simulations well in the SSWM regime (Figure 5, C and E). While they are less accurate outside of the SSWM regime, they nevertheless still produce the correct sign of the evolved correlation within the parameter regimes of our simulations (Figure S6, A–C). However, the signs of the correlations can indeed change depending on the underlying distribution of mutational effects $p_{\text{mut}}(\gamma, \omega, \delta)$. For example, in the Supplemental Methods, we explore the effects of varying the mean mutational effects (Figure S6D)—*e.g.*, whether an average mutation has positive, negative, or zero effect on the growth rate—as well as the intrinsic mutational correlation between the relative growth rate change and the relative lag time change (Figure S6E).

Discussion

We have investigated a model of microbial evolution under serial dilution, which is both a common protocol for laboratory evolution experiments (Luckinbill 1978; Lenski *et al.* 1991; Elena and Lenski 2003; Levy *et al.* 2015; Kram *et al.* 2017) as well as a rough model of evolution in natural environments with feast–famine cycles. While there has been extensive work to model population and evolutionary dynamics in these conditions (Gerrish and Lenski 1998; Wahl and Gerrish 2001; Desai 2013; Baake *et al.* 2019; Guo *et al.* 2019), these models have largely neglected the physiological links connecting mutations to selection. However, models that explicitly incorporate these features are necessary to interpret experimental evidence that mutations readily generate variation in multiple cellular traits, and that this variation is important to adaptation (Vasi *et al.* 1994; Novak *et al.* 2006; Reding-Roman *et al.* 2017; Li *et al.* 2018). Wahl and Zhu (2015) determined the relative fixation probabilities of mutations on different traits and the effects of mutation occurrence time and dilution factor, but the role of pleiotropy and evolutionary dynamics over many mutations were not considered.

In this paper, we have studied a model where mutations can affect three quantitative growth traits—the lag time, the exponential growth rate, and the yield (Figure 1A)—since these three traits are widely measured for microbial populations. In particular, we have derived a simple expression (Equation 3)

for the selection coefficient of a mutation in terms of its effects on growth and lag and a single environmental parameter, the dilution factor D. While previous work showed that this particular form of the selection coefficient determines the fixation probability of a single mutation in the SSWM regime (Manhart *et al.* 2018), here we show that this holds even in the presence of clonal interference (Figure 2, C–F), which appears to be widespread in laboratory evolution experiments (Lang *et al.* 2011, 2013; Good *et al.* 2017). Our result is therefore valuable for interpreting the abundant experimental data on mutant growth traits. We have also calculated the adaptation rates of growth traits per cycle in the SSWM regime, which turn out to increase with the amount of resource R and decrease with the dilution factor D. These results are confirmed by numerical simulations and remain good predictions even outside of the SSWM regime. Furthermore, some of these results are independent of the specific form of the selection coefficient (Equation 3), namely the fact that the fixation probability depends only on the selection coefficient (with other population parameters besides the mutant traits being held fixed) even in the clonal interference regime, and the expressions for the correlation coefficients of traits between populations (Equations 10 and 11).

An important difference with the previous work on this model is that here we used a fixed dilution factor D, which requires that the bottleneck population size N_0 fluctuates as the population evolves. In contrast, previous work used a fixed N_0 and variable D (Manhart *et al.* 2018; Manhart and Shakhnovich 2018). We observed two important differences between these regimes. First, in the case of fixed N_0 and variable D, the fold-change of the population during a single growth cycle, which is approximately $R\bar{Y}/N_0$ (Manhart *et al.* 2018), determines the relative selection between growth and lag, since it determines how long the population undergoes exponential growth. Therefore one can experimentally tune this relative selection by varying either the total amount of resources R or the fixed bottleneck size N_0. However, when the dilution factor D is fixed, the population fold-change is always constrained to exactly equal D, and therefore D alone determines the relative selection on growth and lag (Equation 3). The second difference is that, with fixed N_0 and variable D, the selection coefficient depends explicitly on the effective yield $\bar{Y}$ and is therefore frequency-dependent (Supplemental Methods, section II), which enables the possibility of stable coexistence between two strains (Manhart *et al.* 2018; Manhart and Shakhnovich 2018). However, for the fixed D case, the frequency dependence of $\bar{Y}$ is exactly canceled by N_0 (Equation 4). Therefore, there is only neutral coexistence in this case, requiring the growth and lag traits of the strains to follow an exact constraint set by D (Supplemental Methods, section III).

A major result of our model is a prediction on the evolution of covariation between growth traits. In particular, we have shown that correlations between traits can emerge from selection and accumulation of multiple mutations even without an intrinsic correlation between traits from individual mutations (Figure 5 and Figure S6). We have also shown that selection alone produces no correlation between growth and yield, in the absence of correlated mutational effects (Figure 2B and Figure 3E). This is important for interpreting evolved patterns of traits in terms of selective or physiological tradeoffs. Specifically, it emphasizes that the evolved covariation between traits conflates both the underlying supply of variation from mutations as well as the action of selection and other aspects of population dynamics (*e.g.*, genetic drift, spatial structure, recombination), and therefore it is difficult to make clear inferences about either aspect purely from the outcome of evolution alone. For example, simply observing a negative correlation between two traits from evolved populations is insufficient to infer whether that correlation is due to a physiological constraint on mutations (*e.g.*, mutations cannot improve both traits simultaneously) or due to a selective constraint (*e.g.*, selection favors specialization in one trait or another).

These questions, of course, have been the foundation of quantitative trait genetics (Lynch and Walsh 1998). Historically, this field has emphasized polymorphic populations with abundant recombination as are applicable to plant and animal breeding. However, this regime is quite different from microbial populations, which, at least under laboratory conditions, are often asexual and dominated by linkage between competing mutations (Lang *et al.* 2011, 2013; Good *et al.* 2017). We therefore need a quantitative description of both between-population as well as within-population covariation of traits of microbial populations in this regime. In the present study, we focus on between-population covariation in growth traits, but recent work by Gomez *et al.* (2019) provides insight into the case of within-population covariation. They showed that a tradeoff across individuals within a population evolves between two quantitative traits under positive, additive selection; this suggests that while growth rate and lag time will be negatively correlated across populations (Figure 5, D and E), they should be positively correlated within populations.

Microbial growth traits should indeed be an ideal setting for this approach due to abundant data, but conclusions on the nature of trait covariation have remained elusive. Physiological models have predicted a negative correlation between growth rate and lag time across genotypes (Baranyi and Roberts 1994; Himeoka and Kaneko 2017), while models of single-cell variation in lag times also suggest there should be a negative correlation at the whole-population level (Baranyi 1998). However, experimental evidence has been mixed, with some studies finding a negative correlation (Ziv *et al.* 2013, 2017), while others found no correlation (Levin-Reisman *et al.* 2010; Warringer *et al.* 2011; Adkar *et al.* 2017). Studies of growth–yield correlations have long been motivated by *r/K* selection theory, which suggests there should be tradeoffs between growth rate and yield (Reznick *et al.* 2002). For instance, metabolic models make this prediction (Pfeiffer *et al.* 2001; MacLean 2007; Meyer *et al.* 2015). However, experimental evidence has again been

mixed, with some data showing a tradeoff (Jasmin and Zeyl 2012; Jasmin *et al.* 2012; Bachmann *et al.* 2013), while others show no correlation (Velicer and Lenski 1999; Novak *et al.* 2006; Fitzsimmons *et al.* 2010; Reding-Roman *et al.* 2017) or even a positive correlation (Luckinbill 1978; Warringer *et al.* 2011). Some of this ambiguity may have to do with dependence on the environmental conditions (Reding-Roman *et al.* 2017) or the precise definition of yield. We define yield as the proportionality constant of population size to resource (Equation 1) and neglect any growth rate dependence on resource concentration. Under these conditions, we predict no direct selection on yield, which means that the only way to generate a correlation of yield with growth rate is if the two traits are constrained at the physiological level, so that mutational effects are correlated. In such cases yield could evolve but only as a spandrel (Gould and Lewontin 1979; Amir 2017). Ultimately, we believe more precise single-cell measurements of these traits, both across large unselected mutant libraries as well as evolved strains, are necessary to definitively test these issues (Campos *et al.* 2018).

Acknowledgments

We thank Christine Jacobs-Wagner for kindly sharing the data of single-gene deletions of *E. coli*, and we thank Yipei Guo for suggesting the proof of the sign of the evolved growth rate and lag time correlation presented in the Supplemental Methods. M.M. was supported by an F32 fellowship from the US National Institutes of Health (GM116217) and an Ambizione grant from the Swiss National Science Foundation (PZ00P3_180147). A.A. was supported by National Science Foundation CAREER grant 1752024 and the Harvard Dean's Competitive Fund. A.A. and J.L. received support from Harvard's Materials Research and Engineering Center (DMR-1420570).

Literature Cited

Adkar, B. V., M. Manhart, S. Bhattacharyya, J. Tian, M. Musharbash, *et al.*, 2017 Optimization of lag phase shapes the evolution of a bacterial enzyme. Nat. Ecol. Evol. 1: 149. https://doi.org/10.1038/s41559-017-0149

Amir, A., 2017 Is cell size a spandrel? eLife 6: e22186. https://doi.org/10.7554/eLife.22186

Avrani, S., E. Bolotin, S. Katz, and R. Hershberg, 2017 Rapid genetic adaptation during the first four months of survival under resource exhaustion. Mol. Biol. Evol. 34: 1758–1769. https://doi.org/10.1093/molbev/msx118

Baake, E., A. G. Casanova, S. Probst, and A. Wakolbinger, 2019 Modelling and simulating lenski's long-term evolution experiment. Theor. Popul. Biol. 127: 58–74. https://doi.org/10.1016/j.tpb.2019.03.006

Bachmann, H., M. Fischlechner, I. Rabbers, N. Barfa, F. B. dos Santos *et al.*, 2013 Availability of public goods shapes the evolution of competing metabolic strategies. Proc. Natl. Acad. Sci. USA 110: 14302–14307. https://doi.org/10.1073/pnas.1308523110

Baranyi, J., 1998 Comparison of stochastic and deterministic concepts of bacterial lag. J. Theor. Biol. 192: 403–408. https://doi.org/10.1006/jtbi.1998.0673

Baranyi, J., and T. A. Roberts, 1994 A dynamic approach to predicting bacterial growth in food. Int. J. Food Microbiol. 23: 277–294. https://doi.org/10.1016/0168-1605(94)90157-0

Barrick, J. E., and R. E. Lenski, 2013 Genome dynamics during experimental evolution. Nat. Rev. Genet. 14: 827–839. https://doi.org/10.1038/nrg3564

Barrick, J. E., D. S. Yu, S. H. Yoon, H. Jeong, T. K. Oh *et al.*, 2009 Genome evolution and adaptation in a long-term experiment with Escherichia coli. Nature 461: 1243–1247. https://doi.org/10.1038/nature08480

Campos, M., S. K. Govers, I. Irnov, G. S. Dobihal, F. Cornet *et al.*, 2018 Genomewide phenotypic analysis of growth, cell morphogenesis, and cell cycle events in escherichia coli. Mol. Syst. Biol. 14: e7573. https://doi.org/10.15252/msb.20177573

Chevereau, G., M. Dravecká, T. Batur, A. Guvenek, D. H. Ayhan *et al.*, 2015 Quantifying the determinants of evolutionary dynamics leading to drug resistance. PLoS Biol. 13: e1002299. https://doi.org/10.1371/journal.pbio.1002299

Chevin, L.-M., 2011 On measuring selection in experimental evolution. Biol. Lett. 7: 210–213. https://doi.org/10.1098/rsbl.2010.0580

Crow, J. F., and M. Kimura, 1970 *An Introduction to Population Genetics Theory*. Harper and Row, New York.

Desai, M. M., 2013 Statistical questions in experimental evolution. J. Stat. Mech. 2013: P01003. https://doi.org/10.1088/1742-5468/2013/01/P01003

Desai, M. M., and D. S. Fisher, 2007 Beneficial mutation–selection balance and the effect of linkage on positive selection. Genetics 176: 1759–1798. https://doi.org/10.1534/genetics.106.067678

Elena, S. F., and R. E. Lenski, 2003 Evolution experiments with microorganisms: the dynamics and genetic bases of adaptation. Nat. Rev. Genet. 4: 457–469. https://doi.org/10.1038/nrg1088

Finkel, S. E., 2006 Long-term survival during stationary phase: evolution and the gasp phenotype. Nat. Rev. Microbiol. 4: 113–120. https://doi.org/10.1038/nrmicro1340

Fisher, D. S., 2013 Asexual evolution waves: fluctuations and universality. J. Stat. Mech. 2013: P01011. https://doi.org/10.1088/1742-5468/2013/01/P01011

Fitzsimmons, J. M., S. E. Schoustra, J. T. Kerr, and R. Kassen, 2010 Population consequences of mutational events: effects of antibiotic resistance on the r/K trade-off. Evol. Ecol. 24: 227–236. https://doi.org/10.1007/s10682-009-9302-8

Gerrish, P. J., and R. E. Lenski, 1998 The fate of competing beneficial mutations in an asexual population. Genetica 102–103: 127–144. https://doi.org/10.1023/A:1017067816551

Gillespie, J. H., 1984 Molecular evolution over the mutational landscape. Evolution 38: 1116–1129. https://doi.org/10.1111/j.1558-5646.1984.tb00380.x

Gomez, K., J. Bertram, and J. Masel, 2019 Directional selection rather than functional constraints can shape the G matrix in rapidly adapting asexuals. Genetics 211: 715–729. https://doi.org/10.1534/genetics.118.301685

Good, B. H., and M. M. Desai, 2014 Deleterious passengers in adapting populations. Genetics 198: 1183–1208. https://doi.org/10.1534/genetics.114.170233

Good, B. H., I. M. Rouzine, D. J. Balick, O. Hallatschek, and M. M. Desai, 2012 Distribution of fixed beneficial mutations and the rate of adaptation in asexual populations. Proc. Natl. Acad. Sci. USA 109: 4950–4955. https://doi.org/10.1073/pnas.1119910109

Good, B. H., M. J. McDonald, J. E. Barrick, R. E. Lenski, and M. M. Desai, 2017 The dynamics of molecular evolution over 60,000 generations. Nature 551: 45–50. https://doi.org/10.1038/nature24287

Gould, S. J., and R. C. Lewontin, 1979 The spandrels of San Marco and the Panglossian paradigm: a critique of the adaptationist

programme. Proc. R. Soc. Lond. B Biol. Sci. 205: 581–598. https://doi.org/10.1098/rspb.1979.0086

Guo, Y., M. Vucelja, and A. Amir, 2019 Stochastic tunneling across fitness valleys can give rise to a logarithmic long-term fitness trajectory. Sci. Adv. 5: eaav3842. https://doi.org/10.1126/sciadv.aav3842

Hartl, D. L., and A. G. Clark, 1997 Principles of *P*opulation *G*enetics, Vol. 116. Sinauer Associates, Sunderland, MA.

Himeoka, Y., and K. Kaneko, 2017 Theory for transitions between exponential and stationary phases: universal laws for lag time. Phys. Rev. X 7: 021049.

Jasmin, J.-N., and C. Zeyl, 2012 Life-history evolution and density-dependent growth in experimental populations of yeast. Evolution 66: 3789–3802. https://doi.org/10.1111/j.1558-5646.2012.01711.x

Jasmin, J.-N., M. M. Dillon, and C. Zeyl, 2012 The yield of experimental yeast populations declines during selection. Proc. Biol. Sci. 279: 4382–4388. https://doi.org/10.1098/rspb.2012.1659

Kram, K. E., C. Geiger, W. M. Ismail, H. Lee, H. Tang *et al*., 2017 Adaptation of escherichia coli to long-term serial passage in complex medium: evidence of parallel evolution. mSystems 2: e00192-16.

Kryazhimskiy, S., D. P. Rice, E. R. Jerison, and M. M. Desai, 2014 Microbial evolution. Global epistasis makes adaptation predictable despite sequence-level stochasticity. Science 344: 1519–1522. https://doi.org/10.1126/science.1250939

Lang, G. I., D. Botstein, and M. M. Desai, 2011 Genetic variation and the fate of beneficial mutations in asexual populations. Genetics 188: 647–661. https://doi.org/10.1534/genetics.111.128942

Lang, G. I., D. P. Rice, M. J. Hickman, E. Sodergren, G. M. Weinstock *et al*., 2013 Pervasive genetic hitchhiking and clonal interference in forty evolving yeast populations. Nature 500: 571–574. https://doi.org/10.1038/nature12344

Lenski, R. E., M. R. Rose, S. C. Simpson, and S. C. Tadler, 1991 Long-term experimental evolution in escherichia coli. i. adaptation and divergence during 2,000 generations. Am. Nat. 138: 1315–1341. https://doi.org/10.1086/285289

Levin-Reisman, I., O. Gefen, O. Fridman, I. Ronin, D. Shwa *et al*., 2010 Automated imaging with ScanLag reveals previously undetectable bacterial growth phenotypes. Nat. Methods 7: 737–739. https://doi.org/10.1038/nmeth.1485

Levy, S. F., J. R. Blundell, S. Venkataram, D. A. Petrov, D. S. Fisher *et al*., 2015 Quantitative evolutionary dynamics using high-resolution lineage tracking. Nature 519: 181–186. https://doi.org/10.1038/nature14279

Li, Y., S. Venkataram, A. Agarwala, B. Dunn, D. A. Petrov *et al*., 2018 Hidden complexity of yeast adaptation under simple evolutionary conditions. Curr. Biol. 28: 515–525.e6. https://doi.org/10.1016/j.cub.2018.01.009

Lin, J., and A. Amir, 2017 The effects of stochasticity at the single-cell level and cell size control on the population growth. Cell Syst. 5: 358–367.e4. https://doi.org/10.1016/j.cels.2017.08.015

Luckinbill, L. S., 1978 r and K selection in experimental populations of Escherichia coli. Science 202: 1201–1203. https://doi.org/10.1126/science.202.4373.1201

Lynch, M., and B. Walsh, 1998 *Genetics and Analysis of Quantitative Characters*. Sinauer Associates, Sunderland, MA.

MacLean, R. C., 2007 The tragedy of the commons in microbial populations: insights from theoretical, comparative and experimental studies. Heredity 100: 471–477. https://doi.org/10.1038/sj.hdy.6801073x

Manhart, M., and E. I. Shakhnovich, 2018 Growth tradeoffs produce complex microbial communities on a single limiting resource. Nat. Commun. 9: 3214. https://doi.org/10.1038/s41467-018-05703-6

Manhart, M., B. V. Adkar, and E. I. Shakhnovich, 2018 Trade-offs between microbial growth phases lead to frequency-dependent and non-transitive selection. Proc. Biol. Sci. 285: 20172459. https://doi.org/10.1098/rspb.2017.2459

Meyer, J. R., I. Gudelj, and R. Beardmore, 2015 Biophysical mechanisms that maintain biodiversity through trade-offs. Nat. Commun. 6: 6278. https://doi.org/10.1038/ncomms7278

Novak, M., T. Pfeiffer, R. E. Lenski, U. Sauer, and S. Bonhoeffer, 2006 Experimental tests for an evolutionary trade-off between growth rate and yield in E. coli. Am. Nat. 168: 242–251. https://doi.org/10.1086/506527

Pfeiffer, T., S. Schuster, and S. Bonhoeffer, 2001 Cooperation and competition in the evolution of ATP-producing pathways. Science 292: 504–507. https://doi.org/10.1126/science.1058079

Reding-Roman, C., M. Hewlett, S. Duxbury, F. Gori, I. Gudelj, *et al*., 2017 The unconstrained evolution of fast and efficient antibiotic-resistant bacterial genomes. Nat. Ecol. Evol. 1: 50. https://doi.org/10.1038/s41559-016-0050

Reznick, D., M. J. Bryant, and F. Bashey, 2002 r- and K-selection revisited: the role of population regulation in life-history evolution. Ecology 83: 1509–1520. https://doi.org/10.1890/0012-9658(2002)083[1509:RAKSRT]2.0.CO;2

Schiffels, S., G. J. Szöllősi, V. Mustonen, and M. Lässig, 2011 Emergent neutrality in adaptive asexual evolution. Genetics 189: 1361–1375. https://doi.org/10.1534/genetics.111.132027

Simpson, E. H., 1951 The interpretation of interaction in contingency tables. J. R. Stat. Soc. B 13: 238–241.

Smith, H. L., 2011 Bacterial competition in serial transfer culture. Math. Biosci. 229: 149–159. https://doi.org/10.1016/j.mbs.2010.12.001

Vasi, F., M. Travisano, and R. E. Lenski, 1994 Long-term experimental evolution in Escherichia coli. II. changes in life-history traits during adaptation to a seasonal environment. Am. Nat. 144: 432–456. https://doi.org/10.1086/285685

Velicer, G. J., and R. E. Lenski, 1999 Evolutionary trade-offs under conditions of resource abundance and scarcity: experiments with bacteria. Ecology 80: 1168–1179. https://doi.org/10.1890/0012-9658(1999)080[1168:ETOUCO]2.0.CO;2

Wahl, L. M., and P. J. Gerrish, 2001 The probability that beneficial mutations are lost in populations with periodic bottlenecks. Evolution 55: 2606–2610. https://doi.org/10.1111/j.0014-3820.2001.tb00772.x

Wahl, L. M., and A. D. Zhu, 2015 Survival probability of beneficial mutations in bacterial batch culture. Genetics 200: 309–320. https://doi.org/10.1534/genetics.114.172890

Warringer, J., E. Zörgö, F. A. Cubillos, A. Zia, A. Gjuvsland *et al*., 2011 Trait variation in yeast is defined by population history. PLoS Genet. 7: e1002111. https://doi.org/10.1371/journal.pgen.1002111

Wielgoss, S., J. E. Barrick, O. Tenaillon, S. Cruveiller, B. Chane-Woon-Ming *et al*., 2011 Mutation rate inferred from synonymous substitutions in a long-term evolution experiment with Escherichia coli. G3 (Bethesda) 1: 183–186. https://doi.org/10.1534/g3.111.000406

Wiser, M. J., N. Ribeck, and R. E. Lenski, 2013 Long-term dynamics of adaptation in asexual populations. Science 342: 1364–1367. https://doi.org/10.1126/science.1243357

Zackrisson, M., J. Hallin, L.-G. Ottosson, P. Dahl, E. Fernandez-Parada *et al*., 2016 Scan-o-matic: high-resolution microbial phenomics at a massive scale. G3 (Bethesda) 6: 3003–3014. https://doi.org/10.1534/g3.116.032342

Ziv, N., M. L. Siegal, and D. Gresham, 2013 Genetic and nongenetic determinants of cell growth variation assessed by high-throughput microscopy. Mol. Biol. Evol. 30: 2568–2578. https://doi.org/10.1093/molbev/mst138

Ziv, N., B. M. Shuster, M. L. Siegal, and D. Gresham, 2017 Resolving the complex genetic basis of phenotypic variation and variability of cellular growth. Genetics 206: 1645–1657. https://doi.org/10.1534/genetics.116.195180

Communicating editor: L. Wahl

Supplementary Methods: Evolution of microbial growth traits under serial dilution

Jie Lin,[1] Michael Manhart,[2,3] and Ariel Amir[1]

[1] *John A. Paulson School of Engineering and Applied Sciences, Harvard University, Cambridge, MA 02138, USA*
[2] *Department of Chemistry and Chemical Biology, Harvard University, Cambridge, MA 02138, USA*
[3] *Institute of Integrative Biology, ETH Zurich, 8092 Zurich, Switzerland*

(Dated: May 1, 2020)

I. DETERMINISTIC POPULATION DYNAMICS OVER SERIAL DILUTIONS

At the beginning of the nth growth cycle, let the total population size be $N_0(n)$ and frequency of each strain k be $x_k(n)$. To determine the strain frequencies $\{x_k(n+1)\}$ and the initial population size $N_0(n+1)$ for cycle $n+1$, we first note that the selection coefficients relate the frequencies between consecutive cycles according to

$$s_{ij}(n) = \ln\left(\frac{x_i(n+1)}{x_j(n+1)}\right) - \ln\left(\frac{x_i(n)}{x_j(n)}\right), \tag{S1}$$

which follows from the definition in Eq. 2 and the condition that dilution preserves frequencies, i.e., the frequencies at the end of cycle n equal the frequencies at the beginning of cycle $n+1$ (neglecting stochastic effects of sampling). We can rearrange Eq. S1 to determine the frequencies in cycle $n+1$ as functions of the frequencies in cycle n and the selection coefficients:

$$x_i(n+1) = \frac{x_i(n)}{\sum_{\text{strain } k} x_k(n) e^{s_{ki}(n)}}. \tag{S2}$$

The population size $N_0(n+1)$ for the beginning of cycle $n+1$ is the population size at the end of the nth cycle diluted by D. The total population size at the end of the nth cycle is

$$\begin{aligned}
\sum_{\text{strain } k} N_0(n) x_k(n) e^{r_k(t_c(n)-L_k)} &= \left(\frac{R}{N_0(n)\sum_{\text{strain } \ell} \frac{x_\ell(n)}{Y_\ell} e^{r_\ell(t_c(n)-L_\ell)}}\right) \sum_{\text{strain } k} N_0(n) x_k(n) e^{r_k(t_c(n)-L_k)} \\
&= R\left(\sum_{\text{strain } \ell} \frac{1}{Y_\ell} \frac{x_\ell(n) e^{r_\ell(t_c(n)-L_\ell)}}{\sum_{\text{strain } k} x_k(n) e^{r_k(t_c(n)-L_k)}}\right)^{-1} \\
&= R\left(\sum_{\text{strain } \ell} \frac{1}{Y_\ell} \frac{x_\ell(n)}{\sum_{\text{strain } k} x_k(n) e^{s_{k\ell}(n)}}\right)^{-1} \\
&= R\left(\sum_{\text{strain } \ell} \frac{x_\ell(n+1)}{Y_\ell}\right)^{-1},
\end{aligned} \tag{S3}$$

where we have inserted the quantity in parentheses on the right-hand side of the first line because it equals 1 according to the saturation equation (Eq. 1), and we invoke Eq. S2 to obtain the last line. Therefore the initial population size in cycle $n+1$ equals this quantity diluted by D:

$$N_0(n+1) = \frac{R}{D}\left(\sum_{\text{strain } \ell} \frac{x_\ell(n+1)}{Y_\ell}\right)^{-1}. \tag{S4}$$

Equation S4 shows that the ratio R/D controls the overall magnitude of the bottleneck population size $N_0(n)$, and hence the effective population size for evolutionary dynamics. Furthermore, Eq. S4 indicates that for $n \geq 1$, the effective population yield and initial population size are constrained such that

$$\frac{R\bar{Y}(n)}{N_0(n)} = D, \tag{S5}$$

where we define the effective population yield as

$$\bar{Y}(n) = \left(\sum_{\text{strain } k} \frac{x_k(n)}{Y_k} \right)^{-1}. \tag{S6}$$

II. EQUATIONS FOR SELECTION COEFFICIENTS

Equation 1 in the main text defines the time t_c at which the population exhausts the resource and growth stops; Eq. 2 then defines the selection coefficients s_{ij} in terms of t_c. To determine how all s_{ij} depend explicitly on the parameters of the model, we first rewrite Eq. 2 to get t_c in terms of each s_{ij}:

$$t_c = \frac{s_{ij} + r_i L_i - r_j L_j}{r_i - r_j}. \tag{S7}$$

We then substitute this for t_c in Eq. 1 and rearrange to obtain an implicit nonlinear equation for the selection coefficients s_{ij}:

$$s_{ij} = -\frac{\Delta r_{ij}}{r_i} \ln \left(\frac{N_0}{R} \sum_{\text{strain } k} \frac{x_k}{Y_k} e^{s_{ki}} \right) - \Delta L_{ij} r_j, \tag{S8}$$

where $\Delta r_{ij} = r_i - r_j$ is the difference in growth rates and $\Delta L_{ij} = L_i - L_j$ is the difference in lag times. We can obtain an approximate analytical solution in the limit of weak selection $|s_{ij}| \ll 1$, as shown in previous work [1, 2]:

$$s_{ij} \approx s_{ij}^{\text{lag}} + s_{ij}^{\text{growth}} + \sum_{\text{strain } k} s_{ijk}^{\text{coupling}}, \tag{S9a}$$

where

$$s_{ij}^{\text{lag}} = -\Delta L_{ij} \frac{r_i r_j}{\bar{r}}, \tag{S9b}$$

$$s_{ij}^{\text{growth}} = \frac{\Delta r_{ij}}{\bar{r}} \ln \left(\frac{R\bar{Y}}{N_0} \right), \tag{S9c}$$

$$s_{ijk}^{\text{coupling}} = -\frac{x_k \bar{Y}}{\bar{r} Y_k} (r_i \Delta L_{ik} \Delta r_{kj} - r_j \Delta r_{ik} \Delta L_{kj}), \tag{S9d}$$

are the components of selection on the lag phase, on the growth phase, and on the coupling between lag and growth, and where $\bar{r} = \sum_{\text{strain } k} r_k x_k \frac{\bar{Y}}{Y_k}$ is the effective population growth rate.

III. FREQUENCY-DEPENDENT SELECTION AND COEXISTENCE

In general the selection coefficients are frequency-dependent, meaning they depend not only on the traits of the individual strains (lag times $\{L_k\}$, growth rate $\{r_k\}$, and yields $\{Y_k\}$) but also on their frequencies $\{x_k\}$ at the beginning of the growth cycle. To find the condition for coexistence of all the strains, we set $s_{ij} = 0$ for all pairs of strains i and j in Eq. S8 to obtain

$$0 = -\frac{\Delta r_{ij}}{r_i} \ln \left(\frac{N_0}{R\bar{Y}} \right) - \Delta L_{ij} r_j, \tag{S10}$$

using the definition for the effective population yield $\bar{Y}$ in Eq. S6. Furthermore, since $R\bar{Y}(n)/N_0(n) = D$ for $n \geq 1$ (Eq. S5), the dependence on the frequencies $\{x_k\}$ drops out and we obtain

$$\frac{r_i r_j \Delta L_{ij}}{\Delta r_{ij}} = \ln D. \tag{S11}$$

Geometrically, this means that the lag times $\{L_k\}$ and the reciprocal growth rates $\{1/r_k\}$ for all strains must lie on a straight line, with slope $-\ln D$ (implying a tradeoff between lag and growth) [2]. If this condition is satisfied by all strains, then the population dynamics are neutral at all frequencies $\{x_k\}$. Conversely, if Eq. S11 is not satisfied, the selection coefficients must be nonzero and because Eq. S11 is independent of the frequencies, the selection coefficient can never change sign. Furthermore, previous work showed that the variation in selection coefficients over the range of frequencies tends to be small [1]. Therefore we can approximate the selection on a strain as its selection coefficient at a low mutant frequency, which we do in the next section.

IV. APPROXIMATE SELECTION COEFFICIENT FOR TWO STRAINS

In the two-strain case, we can rewrite the selection coefficient equation (Eq. S8) as

$$s = -\frac{\gamma}{1+\gamma} \ln\left(\frac{N_0}{R}\left[\frac{1-x}{Y_1}e^{-s} + \frac{x}{Y_2}\right]\right) - \omega, \tag{S12}$$

where $s = s_{21}$ is the selection coefficient of the mutant over the wild-type, $\gamma = (r_2 - r_1)/r_1$ is the relative mutant growth rate, $\omega = (L_2 - L_1)r_1$ is the relative mutant lag time, and $x = x_2$ is the mutant frequency. We approximate the selection coefficient by considering the case of mutant being very rare ($x \to 0$), which is the relevant case for the calculation of the fixation probability [3]. In this case we can exactly solve Eq. S12 to obtain

$$\lim_{x\to 0} s = \gamma \ln\left(\frac{RY_1}{N_0}\right) - \omega(1+\gamma). \tag{S13}$$

We invoke the relation $RY_1/N_0 = D$ over serial dilutions (Eq. S5) and drop higher-order terms in γ and ω to finally obtain (Eq. 3)

$$s \approx \gamma \ln D - \omega. \tag{S14}$$

Alternatively, if we assume the selection coefficient s is small in magnitude, we can expand Eq. S12 in s, which yields an identical solution to leading order in γ and ω [1, 2].

V. DISTRIBUTIONS OF MUTATIONAL EFFECTS

When a mutation arises on a background strain with traits r_1, L_1 and Y_1, we randomly generate the new traits r_2, L_2, and Y_2 from a distribution. We assume the changes in traits scale with the values of the background strain's traits, so that the distribution of mutational effects only depends on the relative changes $\gamma = (r_2 - r_1)/r_1$, $\omega = (L_2 - L_1)r_1$, and $\delta = (Y_2 - Y_1)/Y_1$. We ignore epistasis so that mutational effects are additive. In the main text we use a uniform distribution for simplicity:

$$p_{\text{mut}}(\gamma, \omega, \delta) = \begin{cases} (8\gamma_{\max}\omega_{\max}\delta_{\max})^{-1} & \text{for } -\gamma_{\max} < \gamma < \gamma_{\max},\ -\omega_{\max} < \omega < \omega_{\max}, \text{ and } -\delta_{\max} < \delta < \delta_{\max}, \\ 0 & \text{otherwise.} \end{cases} \tag{S15}$$

We use $\gamma_{\max} = 0.02$, $\omega_{\max} = 0.05$, and $\delta_{\max} = 0.02$. In Fig. S6d we generalize this uniform distribution by shifting the mean of γ and ω to nonzero values, so that γ and ω satisfy $-\gamma_{\max} + \mu_\gamma < \gamma < \gamma_{\max} + \mu_\gamma$ and $-\omega_{\max} + \mu_\omega < \omega < \omega_{\max} + \mu_\omega$, where μ_γ and μ_ω are the respective means.

We also consider a Gaussian distribution (Fig. S1 and Fig. S6e), with a potentially nonzero Pearson correlation coefficient ρ_{mut} between growth effects γ and lag effects ω:

$$p_{\text{mut}}(\gamma, \omega, \delta) = \frac{1}{(2\pi)^{3/2}\sigma_\gamma\sigma_\omega\sigma_\delta\sqrt{1-\rho_{\text{mut}}^2}} \exp\left(-\frac{1}{2(1-\rho_{\text{mut}}^2)}\left[\frac{\gamma^2}{\sigma_\gamma^2} + \frac{\omega^2}{\sigma_\omega^2} - \frac{2\rho_{\text{mut}}\gamma\omega}{\sigma_\gamma\sigma_\omega}\right] - \frac{\delta^2}{2\sigma_\delta^2}\right). \tag{S16}$$

VI. EMPIRICAL DISTRIBUTION OF MUTATIONAL EFFECTS IN *E. COLI*

To empirically estimate the distribution of γ, ω, and δ arising from spontaneous mutations, we use data from the Keio collection of single-gene knockouts in *E. coli* [4] as a proxy. Campos et al. [5] measured a population growth curve for each strain in this collection in minimal media with glucose (for example, see Fig. S3a). For each of these mutant growth curves, we infer the growth rate r by fitting the data in the exponential growth phase and then calculate the lag time as $L = t - \ln(N(t)/N(0))/r$, where t is an arbitrary time in the exponential growth phase and $N(t)$ is a proxy for population size (optical density at 600 nm). We also calculate the ratio between the final OD in the stationary phase and the average cell size for each strain; this should be proportional to the total number of cells, and hence also proportional to the yield for a fixed amount of resources. We then determine the mutation's growth rate change $\gamma = (r - r_{\rm wt})/r_{\rm wt}$, lag time change $\omega = (L - L_{\rm wt})r_{\rm wt}$, and yield change $\delta = (Y - Y_{\rm wt})/Y_{\rm wt}$ relative to the wild-type, which has growth rate $r_{\rm wt}$, lag time $L_{\rm wt}$, and yield $Y_{\rm wt}$ averaged over replicates. To correct for plate-dependent effects on these measurements, we follow a prescription determined by the original authors of this data set [5]: we shift all traits in a plate-dependent manner such that the median value of the trait on each plate matches the median value of the trait across all wild-type replicates. Combining this data for all single-gene knockout mutants, we obtain an empirical version of the distribution $p_{\rm mut}(\gamma, \omega, \delta)$ (Fig. S3b,c). For the evolutionary simulations, we restrict $|\gamma| < 0.2$ and $|\omega| < 0.2$ to avoid very large growth rates and negative lag times.

These growth traits are affected by uncertainties due to instrument noise, biological variation across initial inocula, stochastic variation of the growth dynamics, and environmental variation. To estimate the magnitude of this uncertainty, we use 240 growth curves of wild-type replicates from this same data set. Figure S3d,e shows the distributions of growth rates, lag times, and yield proxies of these wild-type replicates along with all mutant strains. The standard deviations of growth rates, lag times, and yield proxies across wild-type replicates are, respectively, 0.0007 $\rm min^{-1}$, 46 min, and 0.0177 $\rm OD/\mu m^3$; for the mutants, they are 0.001 $\rm min^{-1}$, 62 min, and 0.0279 $\rm OD/\mu m^3$. This suggests that many mutant traits are not statistically distinguishable from the wild-type, since they fall within the variation of the wild-type replicates. We can also translate these numbers into rough estimates of minimum values of $|\gamma|$, $|\omega|$, and $|\delta|$ by normalizing by the mean wild-type growth rate (0.009 $\rm min^{-1}$) and mean wild-type yield proxy (0.2363 $\rm OD/\mu m^3$). This indicates that minimum distinguishable $|\gamma|$, $|\omega|$, and $|\delta|$ are approximately 0.08, 0.4 and 0.08, respectively.

VII. ESTIMATING OF THE FIXATION PROBABILITY FROM SIMULATIONS

To calculate the fixation probabilities as functions of γ and ω, we first discretize the space of relative growth rates γ and relative lag times ω (e.g., Fig. 2a). In each bin we calculate the fixation probability as the ratio between the total number of fixed mutations and the total number of mutations that arose in that bin, across 1000 independent populations. We run each simulation for 5000 growth cycles. To ensure the results are independent of the initial conditions, we collect fixation statistics based only on the last 2500 cycles; the results remain the same if we instead only use the last 1250 cycles.

For the uniform distribution of mutational effects (Eq. S15), we use bin sizes of 0.004 for γ and 0.01 for ω (Fig. 2). For the Gaussian distribution (Eq. S16), we use bins of 0.02 for both γ and ω (Fig. S1). Because the ranges of γ and ω of fixed mutations in the Gaussian case are broader than they are in the uniform case, the resulting fixation probabilities are noisier. However, we do not see any systematic effect on the fixation probability from varying the correlation coefficient between γ and ω (Fig. S1).

In Fig. S4a, we further verify the robustness of the fixation probability dependence on the selection coefficient $s = \gamma \ln D - \omega$ by coloring each point according to its neutral phenotype $t = \gamma/\ln D + \omega$ (orthogonal to the selection coefficient s); this quantifies the range of trait combinations that nevertheless have the same selection coefficient and fixation probability. We also plot the fixation probability against the partial selection coefficient $s = \gamma \ln D$ (component of selection on growth alone) in Fig. S4b, which shows that this component of selection alone is insufficient to determine fixation probability.

VIII. FIXATION PROBABILITY UNDER SERIAL DILUTION IN THE SSWM REGIME

Here we calculate the fixation probability of a mutation in the strong-selection weak-mutation (SSWM) regime — where mutations arise and either fix or go extinct one at a time — accounting for serial dilution dynamics (Eq. 5) [6, 7]. The wild-type population has lag time L_1 and growth rate r_1, while the mutant has lag time L_2 and growth rate r_2; the relative growth rate and lag time are therefore $\gamma = (r_2 - r_1)/r_1$ and $\omega = (L_2 - L_1)r_1$, respectively. A single mutant present at the beginning of the growth cycle has fixation probability $2s \approx 2(\gamma \ln D - \omega)$ (Eq. 3), since the dynamics of the mutant and wild-type across growth cycles is mathematically equivalent to a Wright-Fisher process [1, 8].

However, in general mutants will arise sometime in the middle of the growth cycle since they are tied to cell division events. In that case, the fixation probability of a mutation acquires a correction due to the time it arises during that first growth cycle.

Let the total time of the growth cycle be t_c; we assume the saturation time for the first cycle in which the mutant appears is dictated entirely by the wild-type, so that $t_c = L_1 + r_1^{-1} \ln D$. Suppose the mutant arises at time t such that $L_1 < t < L_1 + r_1^{-1} \ln D$. Therefore the number of mutant cells at the end of this first cycle is $e^{r_2(L_1 + r_1^{-1} \ln D - t)}$. The average number of mutant cells at the beginning of the next cycle is simply the number at the end of the previous cycle divided by the dilution factor D. The fixation probability of each of these mutants at the beginning of the next cycle is then given by $2(\gamma \ln D - \omega)$. Assuming $2(\gamma \ln D - \omega)$ is small, the total fixation probability of the original mutant arising at time t is

$$\begin{aligned} \phi_{\mathrm{SSWM}}(\gamma, \omega | t) &= 2(\gamma \ln D - \omega) \frac{e^{r_2(L_1 + r_1^{-1} \ln D - t)}}{D} \\ &= 2(\gamma \ln D - \omega) D^{\gamma} e^{-r_2(t - L_1)}. \end{aligned} \tag{S17}$$

The fixation probability of a mutant therefore decreases exponentially as it occurs later in the growth cycle, since it takes less advantage of that first cycle. Note that if $t = L_1$, i.e., the mutation arises immediately at the beginning of growth, then the fixation probability should be exactly $2(\gamma \ln D - \omega)$ but is off by a factor of D^{γ} due to the approximations during the first cycle; however, this contributes only terms higher-order in γ.

We now average this quantity over all times during the growth cycle. The probability density $p_{\mathrm{arise}}(t)$ of a mutation arising at time t is the rate at which the wild-type population produces mutants per unit time, $\mu r_1 N(t) = \mu r_1 N_0 e^{r_1(t - L_1)}$, divided by the total number of mutants in the growth cycle:

$$\begin{aligned} p_{\mathrm{arise}}(t) &= \frac{\mu r_1 N_0 e^{r_1(t - L_1)}}{\int_{L_1}^{L_1 + r_1^{-1} \ln D} dt \; \mu r_1 N_0 e^{r_1(t - L_1)}} \\ &= \frac{r_1 e^{r_1(t - L_1)}}{D - 1}. \end{aligned} \tag{S18}$$

Therefore the average fixation probability is

$$\begin{aligned} \phi_{\mathrm{SSWM}}(\gamma, \omega) &= \int_{L_1}^{L_1 + r_1^{-1} \ln D} dt \; \phi_{\mathrm{SSWM}}(\gamma, \omega | t) p_{\mathrm{arise}}(t) \\ &= 2(\gamma \ln D - \omega) \frac{D^{\gamma} - 1}{\gamma (D - 1)} \\ &\approx \frac{2 \ln D}{D - 1} (\gamma \ln D - \omega) \left(1 + \gamma \frac{\ln D}{2} \right), \end{aligned} \tag{S19}$$

where on the last line we have kept terms only to second order in γ. The leading-order component is the SSWM fixation probability used in the main text (Eq. 5), where $\ln D/(D-1)$ is the overall correction factor due to the distribution of mutation occurrence times during the growth cycle. Equation S19 furthermore shows that mutations affecting growth rate have an additional benefit over mutations affecting just lag time, since they gain an advantage even in the first cycle (lag time mutations do not have an effect until the next growth cycle) [7, 9]. We note that this calculation is merely an estimate of this effect, since we neglect other corrections second-order in γ and ω, but it nevertheless shows that this effect is at most of order $O(s^2)$.

IX. DISTRIBUTION OF FIXED MUTATIONAL EFFECTS IN THE SSWM REGIME

In the SSWM regime, the probability of fixing a mutation with effects γ and ω conditioned on the event of some mutation fixing is

$$P_{\mathrm{fixed}}(\gamma, \omega) = \frac{1}{Z} p_{\mathrm{mut}}(\gamma, \omega) \phi_{\mathrm{SSWM}}(\gamma \ln D - \omega), \tag{S20}$$

where $p_{\mathrm{mut}}(\gamma,\omega)$ is the probability of a mutation with effects γ and ω arising, and the probability of the mutation fixing is (Eq. 5)

$$\phi_{\mathrm{SSWM}}(s) = \frac{2\ln D}{D-1} s\Theta(s), \tag{S21}$$

where $\Theta(s)$ is the Heaviside theta function. We approximate the selection coefficient of the mutation as $s = \gamma \ln D - \omega$ (Eq. 3 or Eq. S14). The normalization factor is Z, the probability that a randomly chosen mutation fixes:

$$Z = \int d\gamma \int d\omega \; p_{\mathrm{mut}}(\gamma,\omega)\phi_{\mathrm{SSWM}}(\gamma \ln D - \omega). \tag{S22}$$

To calculate moments of the growth rate effect γ and lag time effect ω of fixed mutations, we must take averages over this distribution. That is, we can calculate the mean value of a function $f(\gamma,\omega)$ as

$$\langle f(\gamma,\omega)\rangle_{\mathrm{fixed}} = \int d\gamma \int d\omega \; P_{\mathrm{fixed}}(\gamma,\omega) f(\gamma,\omega). \tag{S23}$$

A. Uniform distribution of mutations

We first consider the case where mutational effects have a uniform distribution (Eq. S15). The normalization factor is

$$\begin{aligned} Z &= \int_{-\gamma_{\max}}^{\gamma_{\max}} d\gamma \int_{-\omega_{\max}}^{\omega_{\max}} d\omega \left(\frac{1}{4\gamma_{\max}\omega_{\max}}\right)\left(\frac{2\ln D}{D-1}\right)(\gamma \ln D - \omega)\Theta(\gamma \ln D - \omega) \\ &= \begin{cases} \dfrac{3\gamma_{\max}^2 \ln^2 D + \omega_{\max}^2}{6\gamma_{\max}(D-1)} & \text{if } \gamma_{\max}\ln D > \omega_{\max}, \\ \dfrac{(\gamma_{\max}^2 \ln^2 D + 3\omega_{\max}^2)\ln D}{6\omega_{\max}(D-1)} & \text{if } \gamma_{\max}\ln D < \omega_{\max}. \end{cases} \end{aligned} \tag{S24}$$

Therefore the moments of γ and ω are (carrying out integrals in a manner similar to Eq. S24)

$$\langle\gamma\rangle_{\text{fixed}} = \begin{cases} \dfrac{2\gamma_{\max}^3 \ln^2 D}{3\gamma_{\max}^2 \ln^2 D + \omega_{\max}^2} & \text{if } \gamma_{\max} \ln D > \omega_{\max}, \\ \dfrac{2\gamma_{\max}^2 \omega_{\max} \ln D}{\gamma_{\max}^2 \ln^2 D + 3\omega_{\max}^2} & \text{if } \gamma_{\max} \ln D < \omega_{\max}, \end{cases} \tag{S25a}$$

$$\langle\omega\rangle_{\text{fixed}} = \begin{cases} -\dfrac{2\gamma_{\max}\omega_{\max}^2 \ln D}{3\gamma_{\max}^2 \ln^2 D + \omega_{\max}^2} & \text{if } \gamma_{\max} \ln D > \omega_{\max}, \\ -\dfrac{2\omega_{\max}^3}{\gamma_{\max}^2 \ln^2 D + 3\omega_{\max}^2} & \text{if } \gamma_{\max} \ln D < \omega_{\max}. \end{cases} \tag{S25b}$$

$$\langle\gamma^2\rangle_{\text{fixed}} = \begin{cases} \dfrac{15\gamma_{\max}^4 \ln^4 D + \omega_{\max}^4}{10(\ln^2 D)(3\gamma_{\max}^2 \ln^2 D + \omega_{\max}^2)} & \text{if } \gamma_{\max} \ln D > \omega_{\max}, \\ \dfrac{1}{5}\gamma_{\max}^2 \left(3 - \dfrac{4\omega_{\max}^2}{\gamma_{\max}^2 \ln^2 D + 3\omega_{\max}^2}\right) & \text{if } \gamma_{\max} \ln D < \omega_{\max}, \end{cases} \tag{S25c}$$

$$\langle\omega^2\rangle_{\text{fixed}} = \begin{cases} \dfrac{1}{15}\omega_{\max}^2 \left(5 + \dfrac{4\omega_{\max}^2}{3\gamma_{\max}^2 \ln^2 D + \omega_{\max}^2}\right) & \text{if } \gamma_{\max} \ln D > \omega_{\max}, \\ \dfrac{\gamma_{\max}^4 \ln^4 D + 15\omega_{\max}^4}{10\left(\gamma_{\max}^2 \ln^2 D + 3\omega_{\max}^2\right)} & \text{if } \gamma_{\max} \ln D < \omega_{\max}, \end{cases} \tag{S25d}$$

$$\langle\gamma\omega\rangle_{\text{fixed}} = \begin{cases} -\dfrac{\omega_{\max}^2(5\gamma_{\max}^2 \ln^2 D - \omega_{\max}^2)}{5(\ln D)(3\gamma_{\max}^2 \ln^2 D + \omega_{\max}^2)} & \text{if } \gamma_{\max} \ln D > \omega_{\max}, \\ -\dfrac{1}{5}\gamma_{\max}^2 (\ln D) \left(\dfrac{8\omega_{\max}^2}{\gamma_{\max}^2 \ln^2 D + 3\omega_{\max}^2} - 1\right) & \text{if } \gamma_{\max} \ln D < \omega_{\max}. \end{cases} \tag{S25e}$$

We can also calculate the variances and covariances:

$$\langle\gamma^2\rangle_{\text{fixed}} - \langle\gamma\rangle_{\text{fixed}}^2 = \begin{cases} \dfrac{5\gamma_{\max}^6 \ln^6 D + 15\gamma_{\max}^4\omega_{\max}^2 \ln^4 D + 3\gamma_{\max}^2\omega_{\max}^4 \ln^2 D + \omega_{\max}^6}{10(\ln^2 D)\left(3\gamma_{\max}^2 \ln^2 D + \omega_{\max}^2\right)^2} & \text{if } \gamma_{\max} \ln D > \omega_{\max}, \\ \dfrac{3\left(\gamma_{\max}^6 \ln^4 D - 2\gamma_{\max}^4\omega_{\max}^2 \ln^2 D + 5\gamma_{\max}^2\omega_{\max}^4\right)}{5\left(\gamma_{\max}^2 \ln^2 D + 3\omega_{\max}^2\right)^2} & \text{if } \gamma_{\max} \ln D < \omega_{\max}, \end{cases} \tag{S26a}$$

$$\langle\omega^2\rangle_{\text{fixed}} - \langle\omega\rangle_{\text{fixed}}^2 = \begin{cases} \dfrac{3\left(5\gamma_{\max}^4\omega_{\max}^2 \ln^4 D - 2\gamma_{\max}^2\omega_{\max}^4 \ln^2 D + \omega_{\max}^6\right)}{5\left(3\gamma_{\max}^2 \ln^2 D + \omega_{\max}^2\right)^2} & \text{if } \gamma_{\max} \ln D > \omega_{\max}, \\ \dfrac{1}{5}\gamma_{\max}^2 (\ln D) \left(1 - \dfrac{8\omega_{\max}^2}{\gamma_{\max}^2 \ln^2 D + 3\omega_{\max}^2}\right) - \dfrac{4\omega_{\max}^6}{\left(\gamma_{\max}^2 \ln^2 D + 3\omega_{\max}^2\right)^2} & \text{if } \gamma_{\max} \ln D < \omega_{\max}, \end{cases} \tag{S26b}$$

$$\langle\gamma\omega\rangle_{\text{fixed}} - \langle\gamma\rangle_{\text{fixed}}\langle\omega\rangle_{\text{fixed}} = \begin{cases} \dfrac{\omega_{\max}^2\left(5\gamma_{\max}^4 \ln^4 D - 2\gamma_{\max}^2\omega_{\max}^2 \ln^2 D + \omega_{\max}^4\right)}{5(\ln D)\left(3\gamma_{\max}^2 \ln^2 D + \omega_{\max}^2\right)^2} & \text{if } \gamma_{\max} \ln D > \omega_{\max}, \\ \dfrac{4\gamma_{\max}^2\omega_{\max}^4 \ln D}{\left(\gamma_{\max}^2 \ln^2 D + 3\omega_{\max}^2\right)^2} + \dfrac{\omega_{\max}^2\left(\omega_{\max}^2 - 5\gamma_{\max}^2 \ln^2 D\right)}{5(\ln D)\left(3\gamma_{\max}^2 \ln^2 D + \omega_{\max}^2\right)} & \text{if } \gamma_{\max} \ln D < \omega_{\max}. \end{cases} \tag{S26c}$$

B. Gaussian distribution of mutations

We now repeat the calculation for a Gaussian distribution of mutational effects (Eq. S16). The normalization factor is

$$\begin{aligned} Z &= \int_{-\infty}^{\infty} d\gamma \int_{-\infty}^{\infty} d\omega \left(\frac{1}{2\pi\sigma_\gamma\sigma_\omega}\exp\left(-\frac{\gamma^2}{2\sigma_\gamma^2}-\frac{\omega^2}{2\sigma_\omega^2}\right)\right)\left(\frac{2\ln D}{D-1}\right)(\gamma\ln D-\omega)\Theta(\gamma\ln D-\omega) \\ &= \int_{-\infty}^{\infty} d\gamma \int_{-\infty}^{\gamma\ln D} d\omega \left(\frac{1}{2\pi\sigma_\gamma\sigma_\omega}\exp\left(-\frac{\gamma^2}{2\sigma_\gamma^2}-\frac{\omega^2}{2\sigma_\omega^2}\right)\right)\left(\frac{2\ln D}{D-1}\right)(\gamma\ln D-\omega) \\ &= \frac{2\ln D}{D-1}\sqrt{\frac{\sigma_\gamma^2\ln^2 D+\sigma_\omega^2}{2\pi}}. \end{aligned} \tag{S27}$$

Therefore the moments of γ and ω are (carrying out integrals in a manner similar to Eq. S27)

$$\langle\gamma\rangle_{\text{fixed}} = \frac{\sigma_\gamma^2\ln D}{2}\sqrt{\frac{2\pi}{\sigma_\gamma^2\ln^2 D+\sigma_\omega^2}}, \tag{S28a}$$

$$\langle\omega\rangle_{\text{fixed}} = -\frac{\sigma_\omega^2}{2}\sqrt{\frac{2\pi}{\sigma_\gamma^2\ln^2 D+\sigma_\omega^2}}, \tag{S28b}$$

$$\langle\gamma^2\rangle_{\text{fixed}} = \sigma_\gamma^2\left(2-\frac{\sigma_\omega^2}{\sigma_\gamma^2\ln^2 D+\sigma_\omega^2}\right), \tag{S28c}$$

$$\langle\omega^2\rangle_{\text{fixed}} = \sigma_\omega^2\left(1+\frac{\sigma_\omega^2}{\sigma_\gamma^2\ln^2 D+\sigma_\omega^2}\right), \tag{S28d}$$

$$\langle\gamma\omega\rangle_{\text{fixed}} = -\frac{\sigma_\gamma^2\sigma_\omega^2\ln D}{\sigma_\gamma^2\ln^2 D+\sigma_\omega^2}. \tag{S28e}$$

The variances and covariances are

$$\langle\gamma^2\rangle_{\text{fixed}} - \langle\gamma\rangle_{\text{fixed}}^2 = \sigma_\gamma^2\left(1-\frac{(\pi-2)\sigma_\gamma^2\ln^2 D)}{2(\sigma_\gamma^2\ln^2 D+\sigma_\omega^2)}\right), \tag{S29a}$$

$$\langle\omega^2\rangle_{\text{fixed}} - \langle\omega\rangle_{\text{fixed}}^2 = \sigma_\omega^2\left(1-\frac{(\pi-2)\sigma_\omega^2}{2(\sigma_\gamma^2\ln^2 D+\sigma_\omega^2)}\right), \tag{S29b}$$

$$\langle\gamma\omega\rangle_{\text{fixed}} - \langle\gamma\rangle_{\text{fixed}}\langle\omega\rangle_{\text{fixed}} = \frac{(\pi-2)\sigma_\gamma^2\sigma_\omega^2\ln D}{2(\sigma_\gamma^2\ln^2 D+\sigma_\omega^2)}. \tag{S29c}$$

C. A general proof on the sign of $\langle\gamma\omega\rangle_{\text{fixed}}$

The quantity $\langle\gamma\omega\rangle_{\text{fixed}}$ is negative for both the uniform (Eq. S25e) and Gaussian (Eq. S28e) cases shown above. We now present a general argument (shared by Yipei Guo) that it must be negative for any distribution of mutational effects $p_{\text{mut}}(\gamma,\omega)$ such that γ and ω are independent ($p_{\text{mut}}(\gamma,\omega) = p_{\text{mut,growth}}(\gamma)p_{\text{mut,lag}}(\omega)$) and the distribution is symmetric around zero ($p_{\text{mut,growth}}(\gamma) = p_{\text{mut,growth}}(-\gamma)$ and $p_{\text{mut,lag}}(\omega) = p_{\text{mut,lag}}(-\omega)$). We want to find the sign of the following integral:

$$I = \int_\gamma d\gamma \int_\omega d\omega\ \gamma\omega(\gamma\ln D-\omega)\Theta(\gamma\ln D-\omega)p_{\text{mut,growth}}(\gamma)p_{\text{mut,lag}}(\omega). \tag{S30}$$

Using the symmetry of $p_{\text{mut,growth}}(\gamma)$ and $p_{\text{mut,lag}}(\omega)$, the above integral must be equal to

$$I' = \int_\gamma d\gamma \int_\omega d\omega\ \gamma\omega|\gamma \ln D - \omega|\Theta(\omega - \gamma \ln D)p_{\mathrm{mut,growth}}(\gamma)p_{\mathrm{mut,lag}}(\omega). \tag{S31}$$

Therefore we can rewrite I and remove the Θ function:

$$I = \frac{1}{2}\int_\gamma d\gamma \int_\omega d\omega\ \gamma\omega|\gamma \ln D - \omega|p_{\mathrm{mut,growth}}(\gamma)p_{\mathrm{mut,lag}}(\omega). \tag{S32}$$

Given any point in the above integral such that $\gamma\omega > 0$, we can find a corresponding point with $\gamma\omega < 0$ with equal or higher $|\gamma \ln(D) - \omega|$ that occurs with the same probability. Therefore the total integral, and hence $\langle\gamma\omega\rangle_{\mathrm{fixed}}$, must be negative.

X. ADAPTATION RATES OF THE GROWTH RATE AND LAG TIME IN THE SSWM REGIME

In this section, we calculate the average adaptation speeds of growth rate and lag time using the average changes in these traits determined in Sec. IX. First, the total number of cell divisions in a growth cycle is the population size at the end of the cycle, $N_{\mathrm{final}} = \sum_{\mathrm{strain}\ i} N_i(t_c)$, minus the population size at the beginning, N_0. We can approximate the final population size as RY_0, which assumes that the yields of the evolved strains do not vary significantly from the ancestral yield Y_0 (as confirmed by simulations, e.g., Fig. 3e); we also assume $D \gg 1$ so that $N_{\mathrm{final}} - N_0 \approx N_{\mathrm{final}}$. Therefore the total number of mutation events per growth cycle is approximately μRY_0. For each mutation, the average probability that it fixes is Z (Eq. S22). The expected change in growth rate for a mutation is approximately $\langle\gamma\rangle_{\mathrm{fixed}} r_0$, assuming a small number of fixed mutations so that the growth rate has not changed significantly from the ancestral growth rate r_0; similarly, the expected change in lag time is approximately $\langle\omega\rangle_{\mathrm{fixed}}/r_0$.

We find that for both the uniform and Gaussian distributions of mutations, the expected changes in growth rate and lag time per cycle are (Eq. 8)

$$\begin{aligned} W_{\mathrm{growth}} &= \mu RY_0 Z\langle\gamma\rangle_{\mathrm{fixed}} r_0 \\ &= \sigma_\gamma^2 r_0(\ln D)\left(\frac{\mu RY_0 \ln D}{D-1}\right), \end{aligned} \tag{S33}$$

$$\begin{aligned} W_{\mathrm{lag}} &= \mu RY_0 Z\frac{\langle\omega\rangle_{\mathrm{fixed}}}{r_0} \\ &= -\frac{\sigma_\omega^2}{r_0}\left(\frac{\mu RY_0 \ln D}{D-1}\right). \end{aligned} \tag{S34}$$

where $\sigma_\gamma^2 = \gamma_{\max}^2/3$ and $\sigma_\omega^2 = \omega_{\max}^2/3$ are the variances of γ and ω in the case of a uniform distribution (Eq. S15). The ratio between the growth and lag adaptation speeds defines the average direction of evolution in growth-lag trait space (Eq. 9):

$$\frac{W_{\mathrm{growth}}}{W_{\mathrm{lag}}} = -r_0^2\frac{\sigma_\gamma^2}{\sigma_\omega^2}\ln D. \tag{S35}$$

We can use this relation to predict the average trajectory of the population growth rate r_{pop} and lag time L_{pop} over evolution. In the SSWM regime, we can approximate the average population growth rate and lag time as

$$\langle r_{\mathrm{pop}}\rangle = r_0 + nW_{\mathrm{growth}}, \tag{S36}$$

$$\langle L_{\mathrm{pop}}\rangle = L_0 + nW_{\mathrm{lag}}, \tag{S37}$$

where n is the total number of cycles. Therefore,

$$\frac{\langle r_{\mathrm{pop}}\rangle - r_0}{\langle L_{\mathrm{pop}}\rangle - L_0} = -r_0^2\frac{\sigma_\gamma^2}{\sigma_\omega^2}\ln D. \tag{S38}$$

In Fig. S5 we compare this equation with the trajectories obtained from simulations for three values of the dilution factor D. The prediction matches best for large D (Fig. S5a), since that produces smaller population sizes (through Eq. 4) and therefore better approximates the SSWM limit. The prediction becomes less accurate for small D (Fig. S5b,c) when clonal interference plays a larger role, but still matches well at early times.

XI. CORRELATION BETWEEN GROWTH RATES AND LAG TIMES

In this section we calculate the evolved correlations between growth rates and lag times. For a single fixed mutation, the correlation coefficient between the relative change in growth rate γ and relative change in lag time ω is

$$\rho_{\text{fixed}} = \frac{\langle\gamma\omega\rangle_{\text{fixed}} - \langle\gamma\rangle_{\text{fixed}}\langle\omega\rangle_{\text{fixed}}}{\sqrt{\left(\langle\gamma^2\rangle_{\text{fixed}} - \langle\gamma\rangle_{\text{fixed}}^2\right)\left(\langle\omega^2\rangle_{\text{fixed}} - \langle\omega\rangle_{\text{fixed}}^2\right)}}. \tag{S39}$$

However, the quantity more relevant to experimental data is the correlation between absolute growth rate r and lag time L between replicate populations at a given time when multiple mutations have fixed. To calculate this, we focus on the SSWM regime and assume that each mutation has small effects on the growth rate and lag time, so that the total growth rate r and lag time L can be approximated as sums of these effects:

$$\begin{aligned} r &\approx r_0 + r_0 \sum_{i=1}^{m} \gamma_i, \\ L &\approx L_0 + \frac{1}{r_0} \sum_{i=1}^{m} \omega_i, \end{aligned} \tag{S40}$$

where r_0 and L_0 are the ancestral growth rate and lag time, and the sums are over all fixed mutations (indexed by i) up to the total number m.

We can now calculate moments of the evolved growth rate and lag time by averaging over both the distribution of fixed mutations (Eq. S23) and across populations with different numbers m of fixed mutations:

$$\begin{aligned} \overline{\langle Lr\rangle_{\text{fixed}}} &\approx \frac{1}{M} \sum_{\text{population } \alpha} \left\langle \left(r_0 + r_0 \sum_{i=1}^{m_\alpha} \gamma_i\right)\left(L_0 + \frac{1}{r_0}\sum_{i=1}^{m_\alpha}\omega_i\right)\right\rangle_{\text{fixed}} \\ &= \frac{1}{M} \sum_{\text{population } \alpha} \left(r_0 L_0 + m_\alpha \langle\omega\rangle_{\text{fixed}} + L_0 r_0 m_\alpha \langle\gamma\rangle_{\text{fixed}} + m_\alpha \langle\gamma\omega\rangle_{\text{fixed}} + (m_\alpha^2 - m_\alpha)\langle\gamma\rangle_{\text{fixed}}\langle\omega\rangle_{\text{fixed}}\right) \\ &= r_0 L_0 + \overline{m}\langle\omega\rangle_{\text{fixed}} + L_0 r_0 \overline{m}\langle\gamma\rangle_{\text{fixed}} + \overline{m}\langle\gamma\omega\rangle_{\text{fixed}} + (\overline{m^2} - \overline{m})\langle\gamma\rangle_{\text{fixed}}\langle\omega\rangle_{\text{fixed}}. \end{aligned} \tag{S41}$$

Here the bar indicates an average over all independent populations (total number M). Similar calculations yield the (co)variances:

$$\overline{\langle Lr\rangle_{\text{fixed}}} - \overline{\langle L\rangle_{\text{fixed}}}\,\overline{\langle r\rangle_{\text{fixed}}} = \overline{m}\left(\langle\gamma\omega\rangle_{\text{fixed}} - \langle\gamma\rangle_{\text{fixed}}\langle\omega\rangle_{\text{fixed}}\right) + \left(\overline{m^2} - \overline{m}^2\right)\langle\gamma\rangle_{\text{fixed}}\langle\omega\rangle_{\text{fixed}}, \tag{S42}$$

$$\overline{\langle r^2\rangle_{\text{fixed}}} - \left(\overline{\langle r\rangle_{\text{fixed}}}\right)^2 = r_0^2\overline{m}\left(\langle\gamma^2\rangle_{\text{fixed}} - \langle\gamma\rangle_{\text{fixed}}^2\right) + r_0^2\left(\overline{m^2} - \overline{m}^2\right)\langle\gamma\rangle_{\text{fixed}}^2, \tag{S43}$$

$$\overline{\langle L^2\rangle_{\text{fixed}}} - \left(\overline{\langle L\rangle_{\text{fixed}}}\right)^2 = \frac{1}{r_0^2}\overline{m}\left(\langle\omega^2\rangle_{\text{fixed}} - \langle\omega\rangle_{\text{fixed}}^2\right) + \frac{1}{r_0^2}\left(\overline{m^2} - \overline{m}^2\right)\langle\omega\rangle_{\text{fixed}}^2. \tag{S44}$$

That is, the (co)variances of the growth rate and lag time are sums of the (co)variance in the traits for a single fixed mutation and the variance of number of mutations ($\overline{m^2} - \overline{m}^2$). In the SSWM regime, different fixed mutations are independent of each other and the probability of any mutation fixing (Z, Eqs. S24 and S27) is small ($Z \sim D^{-1}$ with $D \gg 1$); therefore the number of fixed mutations over a finite time will be approximately Poisson-distributed, so that the variance approximately equals the mean:

$$\overline{m^2} - \overline{m}^2 \approx \overline{m}. \tag{S45}$$

The Pearson correlation coefficient of the evolved growth rate and lag time is therefore (Eq. 11)

$$\begin{aligned}\rho_{\text{evo}} &= \frac{\overline{\langle Lr\rangle_{\text{fixed}}} - \overline{\langle L\rangle_{\text{fixed}}}\,\overline{\langle r\rangle_{\text{fixed}}}}{\sqrt{\left(\overline{\langle r^2\rangle_{\text{fixed}}} - \left(\overline{\langle r\rangle_{\text{fixed}}}\right)^2\right)\left(\overline{\langle L^2\rangle_{\text{fixed}}} - \left(\overline{\langle L\rangle_{\text{fixed}}}\right)^2\right)}} \\ &\approx \frac{\langle\gamma\omega\rangle_{\text{fixed}}}{\sqrt{\langle\gamma^2\rangle_{\text{fixed}}\langle\omega^2\rangle_{\text{fixed}}}}.\end{aligned} \tag{S46}$$

That is, the correlation between evolved growth and lag depends entirely on the moments of growth and lag for a single fixed mutation, but is not identical to the correlation coefficient for a single fixed mutation (Eq. S39).

For the uniform distribution of mutations (Eq. S15), these two correlations equal:

$$\rho_{\text{fixed}} = \begin{cases} \sqrt{\dfrac{2\omega_{\max}^2(5\gamma_{\max}^4\ln^4 D - 2\gamma_{\max}^2\omega_{\max}^2\ln^2 D + \omega_{\max}^4)}{3(5\gamma_{\max}^6\ln^6 D + 15\gamma_{\max}^4\omega_{\max}^2\ln^4 D + 3\gamma_{\max}^2\omega_{\max}^4\ln^2 D + \omega_{\max}^6)}} & \text{if } \gamma_{\max}\ln D > \omega_{\max}, \\ \dfrac{\left(-5\gamma_{\max}^6\omega_{\max}^2\ln^6 D + 31\gamma_{\max}^4\omega_{\max}^4\ln^4 D - 19\gamma_{\max}^2\omega_{\max}^6\ln^2 D + 9\omega_{\max}^8\right)\left(\sqrt{3}\gamma_{\max}(\ln D)\left(3\gamma_{\max}^2\ln^2 D + \omega_{\max}^2\right)\right)^{-1}}{\sqrt{(\gamma_{\max}^4\ln^4 D - 2\gamma_{\max}^2\omega_{\max}^2\ln^2 D + 5\omega_{\max}^4)(\gamma_{\max}^6\ln^5 D - 2\gamma_{\max}^4\omega_{\max}^2\ln^3 D - 15\gamma_{\max}^2\omega_{\max}^4\ln D - 20\omega_{\max}^6)}} & \text{if } \gamma_{\max}\ln D < \omega_{\max}, \end{cases} \tag{S47a}$$

$$\rho_{\text{evo}} = \begin{cases} -\dfrac{\sqrt{2}\omega_{\max}\left(5\gamma_{\max}^2\ln^2 D - \omega_{\max}^2\right)}{\sqrt{\left(5\gamma_{\max}^2\ln^2 D + 3\omega_{\max}^2\right)\left(15\gamma_{\max}^4\ln^4 D + \omega_{\max}^4\right)}} & \text{if } \gamma_{\max}\ln D > \omega_{\max}, \\ -\dfrac{\omega_{\max}^2\left(\gamma_{\max}^2\ln^2 D + 3\omega_{\max}^2\right)\left(5\gamma_{\max}^2\ln^2 D - \omega_{\max}^2\right)}{\gamma_{\max}^2(\ln D)\left(3\gamma_{\max}^2\ln^2 D + \omega_{\max}^2\right)\sqrt{(\ln D)\left(\gamma_{\max}^2\ln^2 D - 5\omega_{\max}^2\right)\left(3\gamma_{\max}^2\ln^2 D + 5\omega_{\max}^2\right)}} & \text{if } \gamma_{\max}\ln D < \omega_{\max}, \end{cases} \tag{S47b}$$

while for the Gaussian distribution of mutations (Eq. S16) they are

$$\rho_{\text{fixed}} = \frac{(\pi-2)\sigma_\gamma\sigma_\omega\ln D}{\sqrt{\left[(4-\pi)\sigma_\gamma^2\ln^2 D + 2\sigma_\omega^2\right]\left[2\sigma_\gamma^2\ln^2 D + (4-\pi)\sigma_\omega^2\right]}}, \tag{S48a}$$

$$\rho_{\text{evo}} = -\frac{\sigma_\gamma\sigma_\omega\ln D}{\sqrt{2\sigma_\gamma^4\ln^4 D + 5\sigma_\gamma^2\sigma_\omega^2\ln^2 D + 2\sigma_\omega^4}}. \tag{S48b}$$

Note that the correlation ρ_{fixed} for a single fixed mutation is positive in the uniform and Gaussian cases, while the correlation ρ_{evo} between evolved traits is negative (cf. Fig. 5). The latter is true for any independent, symmetric distributions of γ and ω as proved in Sec. IX C.

[1] M. Manhart, B. V. Adkar, and E. I. Shakhnovich, Proc R Soc B **285**, 20172459 (2018).
[2] M. Manhart and E. I. Shakhnovich, Nat Commun **9**, 3214 (2018).
[3] Y. Guo, M. Vucelja, and A. Amir, Sci Adv **5**, eaav3842 (2019).
[4] T. Baba, T. Ara, M. Hasegawa, Y. Takai, Y. Okumura, M. Baba, K. A. Datsenko, M. Tomita, B. L. Wanner, and H. Mori, Mol Syst Biol **2**, 2006.0008 (2006).
[5] M. Campos, S. K. Govers, I. Irnov, G. S. Dobihal, F. Cornet, and C. Jacobs-Wagner, Mol Syst Biol **14**, e7573 (2018).
[6] L. M. Wahl and P. J. Gerrish, Evolution **55**, 2606 (2001).
[7] L. M. Wahl and A. D. Zhu, Genetics **200**, 309 (2015).
[8] J. F. Crow and M. Kimura, An Introduction to Population Genetics Theory (Harper and Row, New York, 1970).
[9] Y. Li, S. Venkataram, A. Agarwala, B. Dunn, D. A. Petrov, G. Sherlock, and D. S. Fisher, Current Biology **28**, 515 (2018).

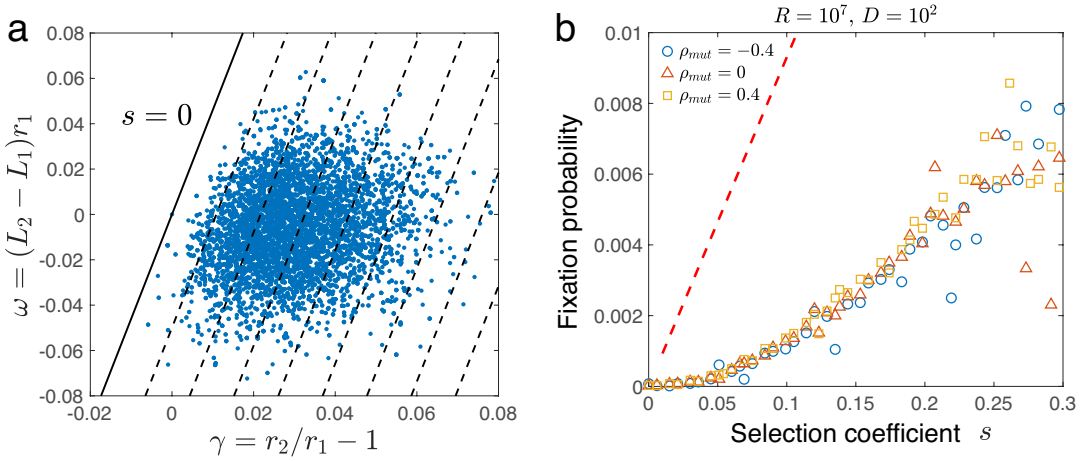

FIG. S1. **Fixation probabilities of mutations with Gaussian-distributed mutational effects** (a) The relative growth rates γ and the relative lag times ω of fixed mutations against their background strain. Dashed lines mark contours of constant selection coefficient with interval $\Delta s = 0.05$ while the solid line marks $s = 0$. The standard deviations of the Gaussian distribution (Eq. S16) are $\sigma_\gamma = \sigma_\omega = \sigma_\delta = 0.02$, with zero correlation ρ_{mut} between γ and ω. The parameters of the population dynamics are $D = 10^2$ and $R = 10^7$. (b) We bin mutations according to their effects γ and ω, and for each bin we calculate the fixation probability and the selection coefficient according to Eq. 3. Different colors represent different growth-lag correlation coefficients ρ_{mut}. The red dashed line shows the fixation probability predicted in the SSWM regime (Eq. 5 in the main text).

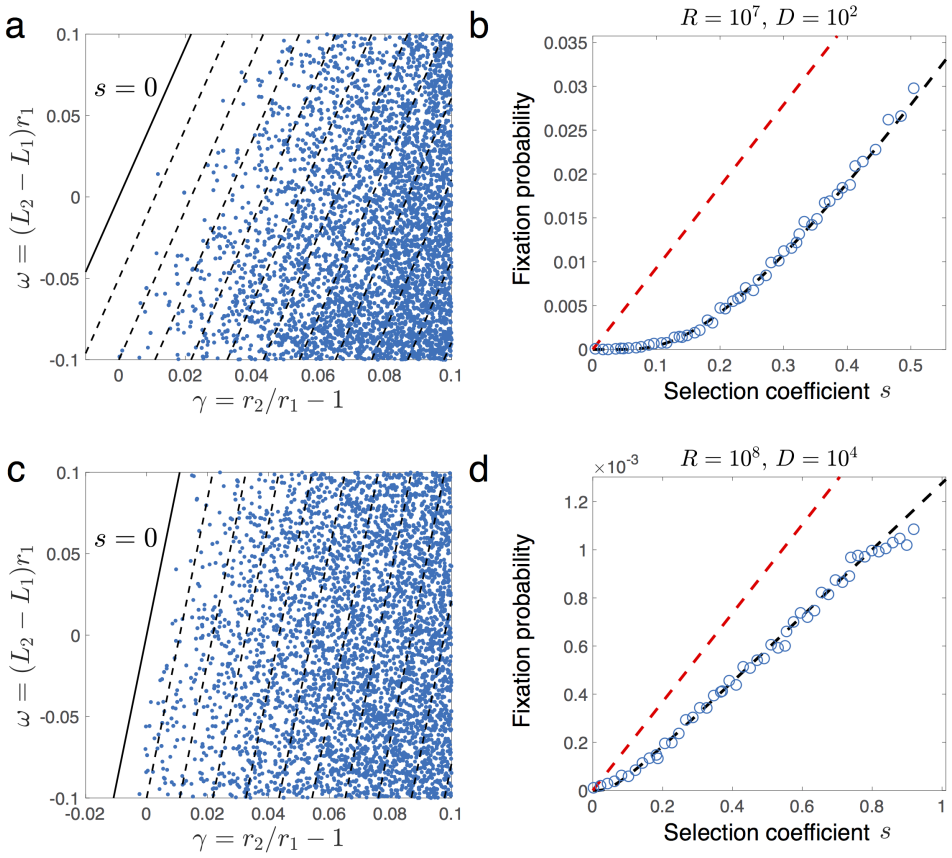

FIG. S2. **Fixation probabilities for large-effect mutations.** (a) The relative growth rate γ and lag time ω of fixed mutations. Dashed lines mark contours of constant selection coefficient with interval $\Delta s = 0.05$, while the solid line marks $s = 0$. The parameters of the population dynamics are $D = 10^2$ and $R = 10^7$. (b) Fixation probability of mutations against their selection coefficient, using fixed mutations from panel (a). The red dashed line shows the fixation probability predicted in the SSWM regime (Eq. 5 in the main text), while the black line shows a numerical fit of the data points to the fixation probability under clonal interference (Eq. 6 in the main text; $A = 0.1072$ and $B = 0.3261$). (c) Same as (a) but for $D = 10^4$ $R = 10^8$ and with $\Delta s = 0.1$. (d) Same as (b) but for fixed mutations in panel (c). Numerical fit of Eq. 6 produces parameters $A = 0.0014$ and $B = 0.0820$. In all panels mutations randomly arise from a uniform distribution $p_{\rm mut}$ where $-0.1 < \gamma < 0.1$ and $-0.1 < \omega < 0.1$, with the mutation rate $\mu = 10^{-6}$ and the distributions of the relative yield δ the same as Fig. 3.

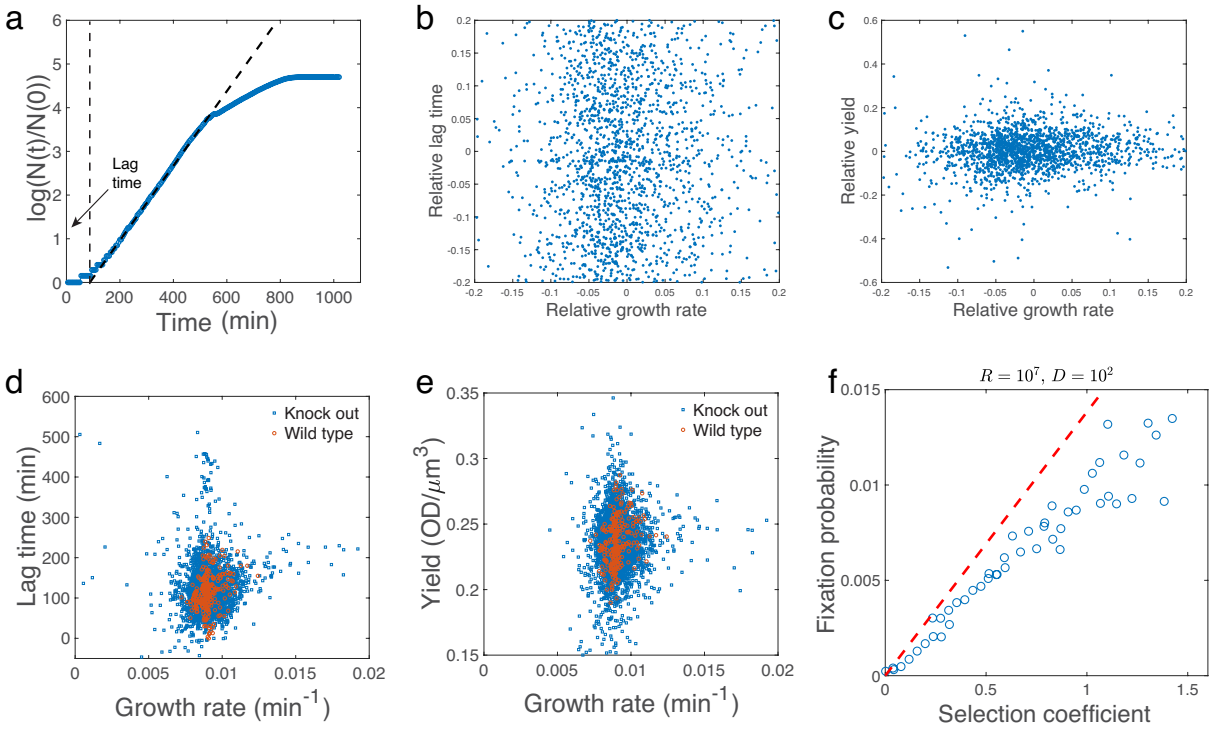

FIG. S3. **Empirical estimate of mutational effects from single-gene knockout collection of *E. coli*.** (a) Example growth curve (optical density at 600 nm) from a single-gene knockout strain (cyoC deleted) from which we estimate the growth rate (slope of diagonal dashed line) and the lag time (vertical dashed line). We obtain a proxy for the yield by taking the maximum optical density and normalizing by the average cell size. (b) Relative growth rates γ and relative lag times ω of all knockout mutants compared to the wild-type. The Pearson correlation coefficient between γ and ω is 0.02 ± 0.05. (c) Relative growth rates γ and relative yields δ of all knockout mutants compared to the wild-type. The Pearson correlation coefficient between γ and δ is 0.09 ± 0.05. (d) Growth rates and lag times for all knockout mutants as well as wild-type replicates in the data set. (e) Growth rates and yields for all knockout mutants as well as wild-type replicates in the data set. (f) Fixation probabilities of mutations as functions of the selection coefficient, using the knockout mutant data as the distribution of mutational effects; other parameters are $R = 10^7$, $D = 10^3$, and $\mu = 5 \times 10^{-7}$. The red dashed line shows the fixation probability predicted in the SSWM regime (Eq. 5). Raw growth curve data is from Campos et al. [5].

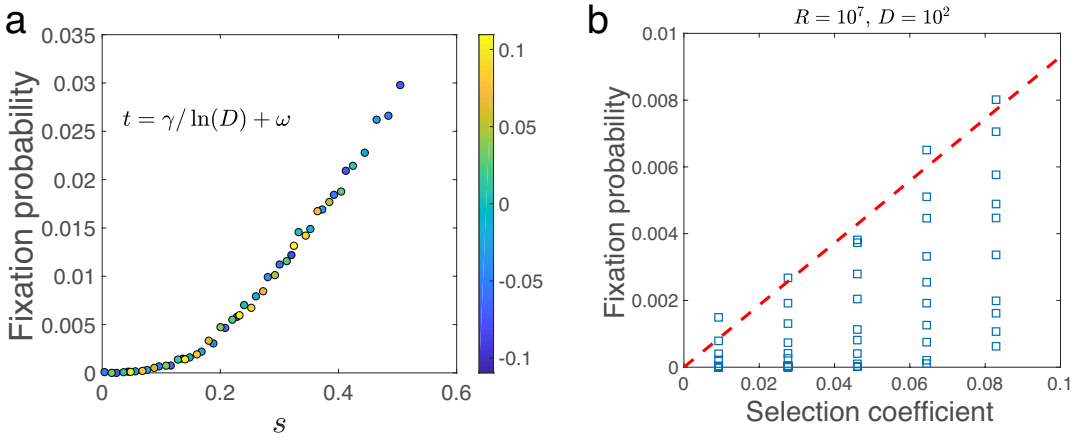

FIG. S4. **Robustness of fixation probability dependence on the selection coefficient.** (a) Fixation probability of mutations as a function of their selection coefficients, but with each data point colored by its neutral phenotype $t = \gamma \ln D + \omega$. The simulation data is the same as in Fig. S2b. (b) We replot Fig. 2e in the main text with the partial selection coefficient $s = \gamma \ln D$ (component of selection of growth alone), which does not lead to a collapse of data.

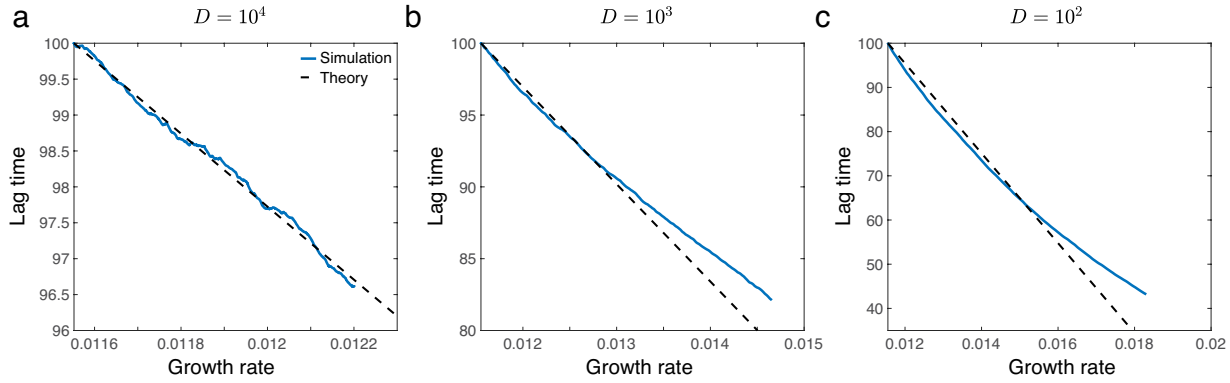

FIG. S5. **Average evolutionary trajectories in growth-lag trait space.** We plot the average population growth rate r_{pop} and lag time L_{pop} from simulations (solid blue lines) with (a) $D = 10^4$, (b) $D = 10^3$, and (c) $D = 10^2$, along with the predicted trajectories in the SSWM limit (Eq. S38; dashed black line). In all panels $R = 10^7$.

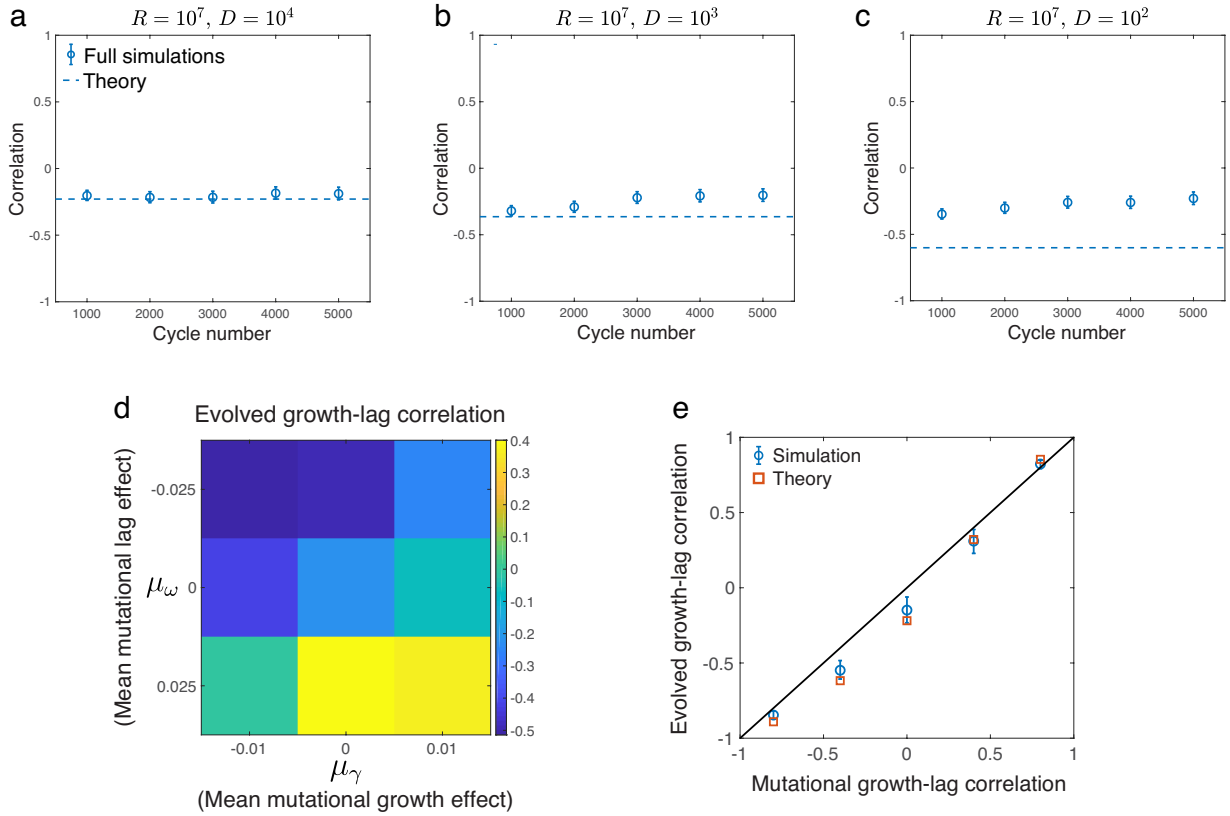

FIG. S6. **Evolved patterns of covaration among growth traits.** (a-c) Pearson correlation coefficients of the population-averaged growth rates and lag times versus the cycle number from simulations. The blue circles are the measured values from the full simulations and the dashed lines are the predictions for the SSWM regime (Eq. 11). The error bars represent 95% confidence intervals. (d) Evolved correlation coefficient ρ_{evo} of growth rate and lag time (after 50000 mutational trials) as a function of the mean mutational effects on growth rate and lag time (Eq. S15). (e) Evolved correlation coefficient ρ_{evo} of growth rate and lag time (after 50000 mutational trials) as a function of the mutational correlation ρ_{mut} of these two traits (Eq. S16). The blue points show simulation results, while the red points show the prediction from Eq. 11. The black line shows the line of identity. In both (d) and (e), we simulate the SSWM regime by introducing random mutations one-by-one and determining their fixation from Eq. 5 with $D = 10^3$.